Wind, SST and upwelling indices

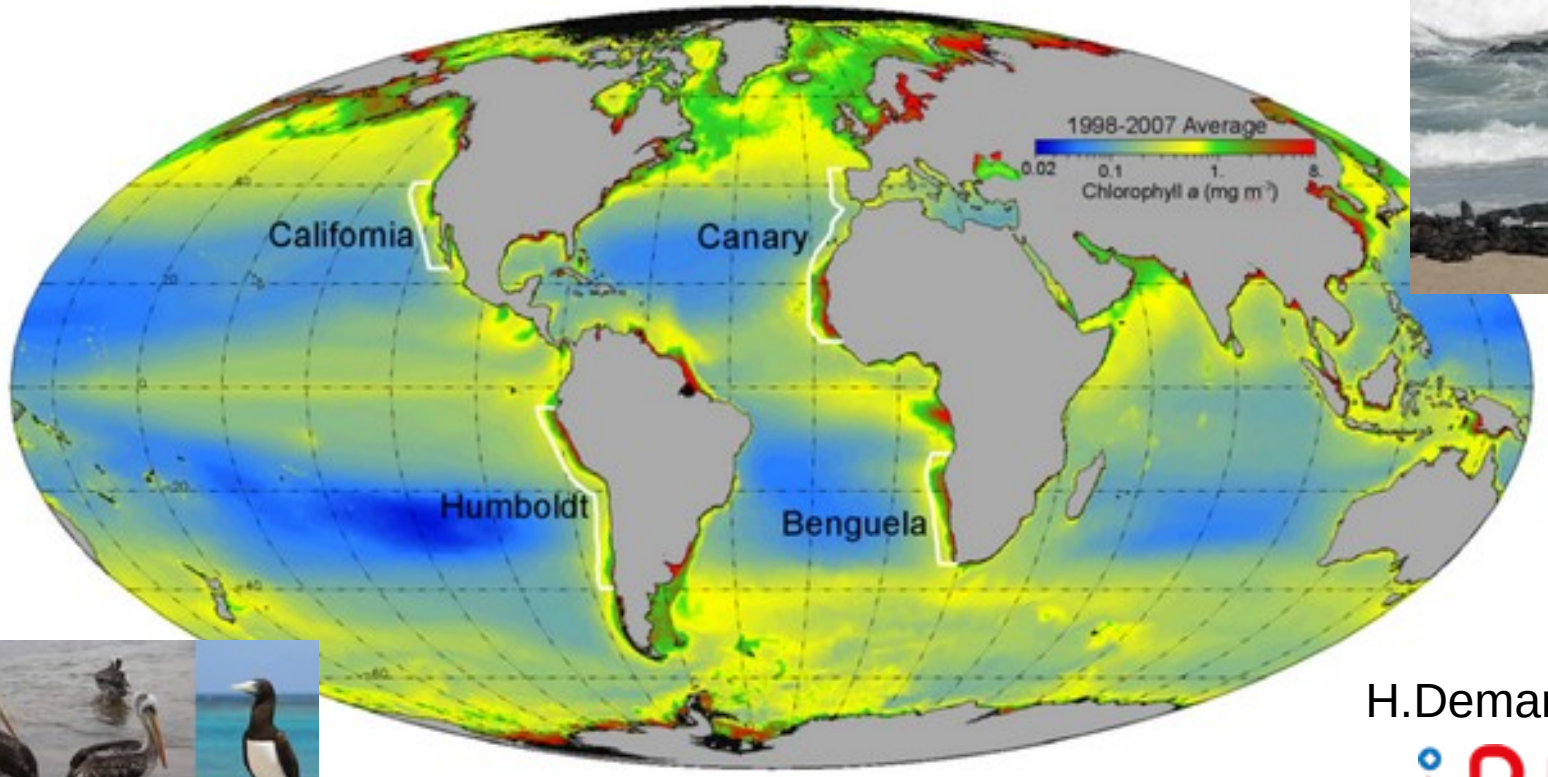

H.Demarcq

Institut de Recherche pour le Développement FRANCE

Ministério da Economia Marítima

OSCM Ocean Science Centre Mindelo

GOBIERNO DE ESPAÑA

Wind, SST and upwelling indices

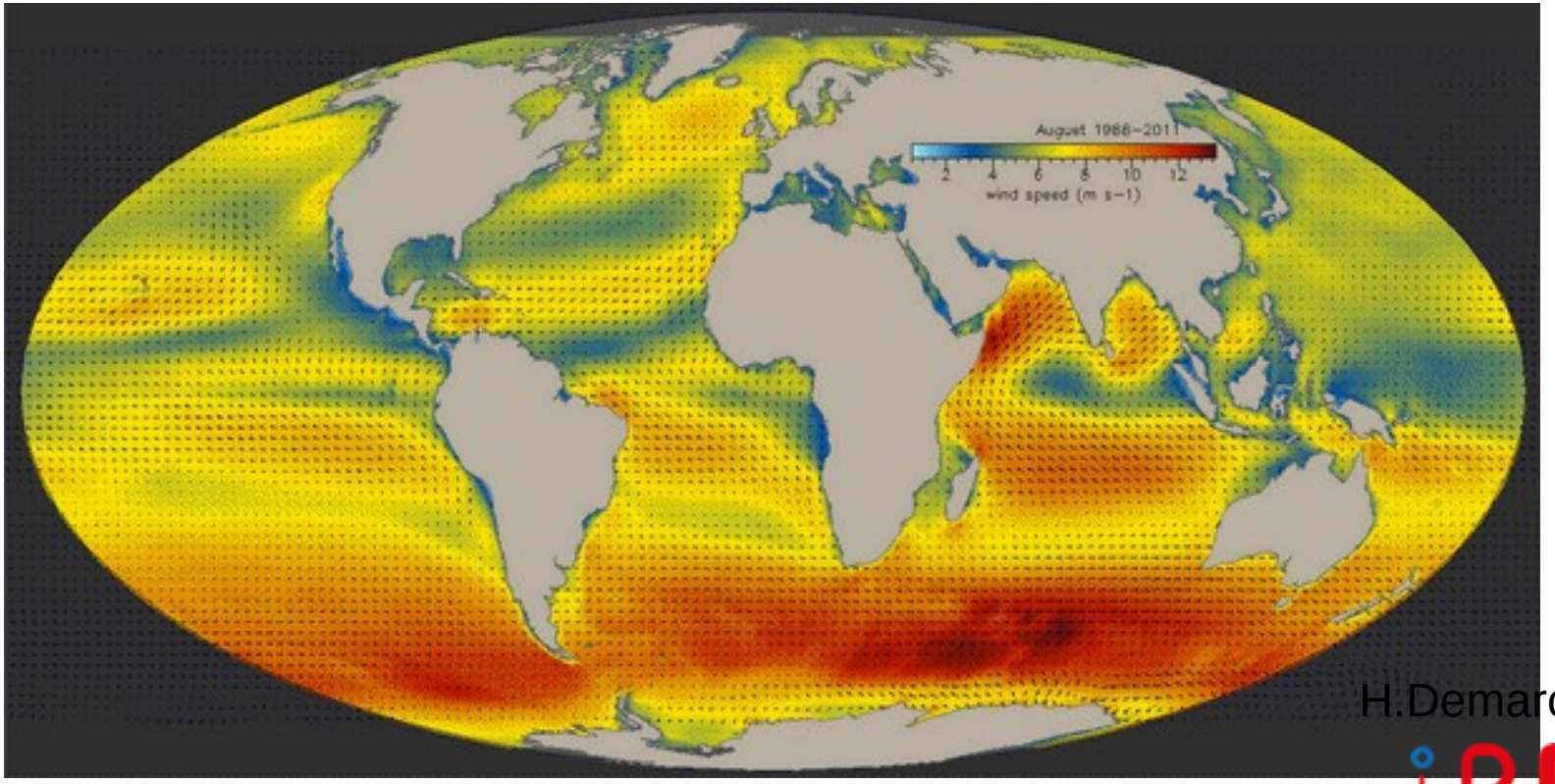

H.Demarcq

Wind, SST and upwelling indices

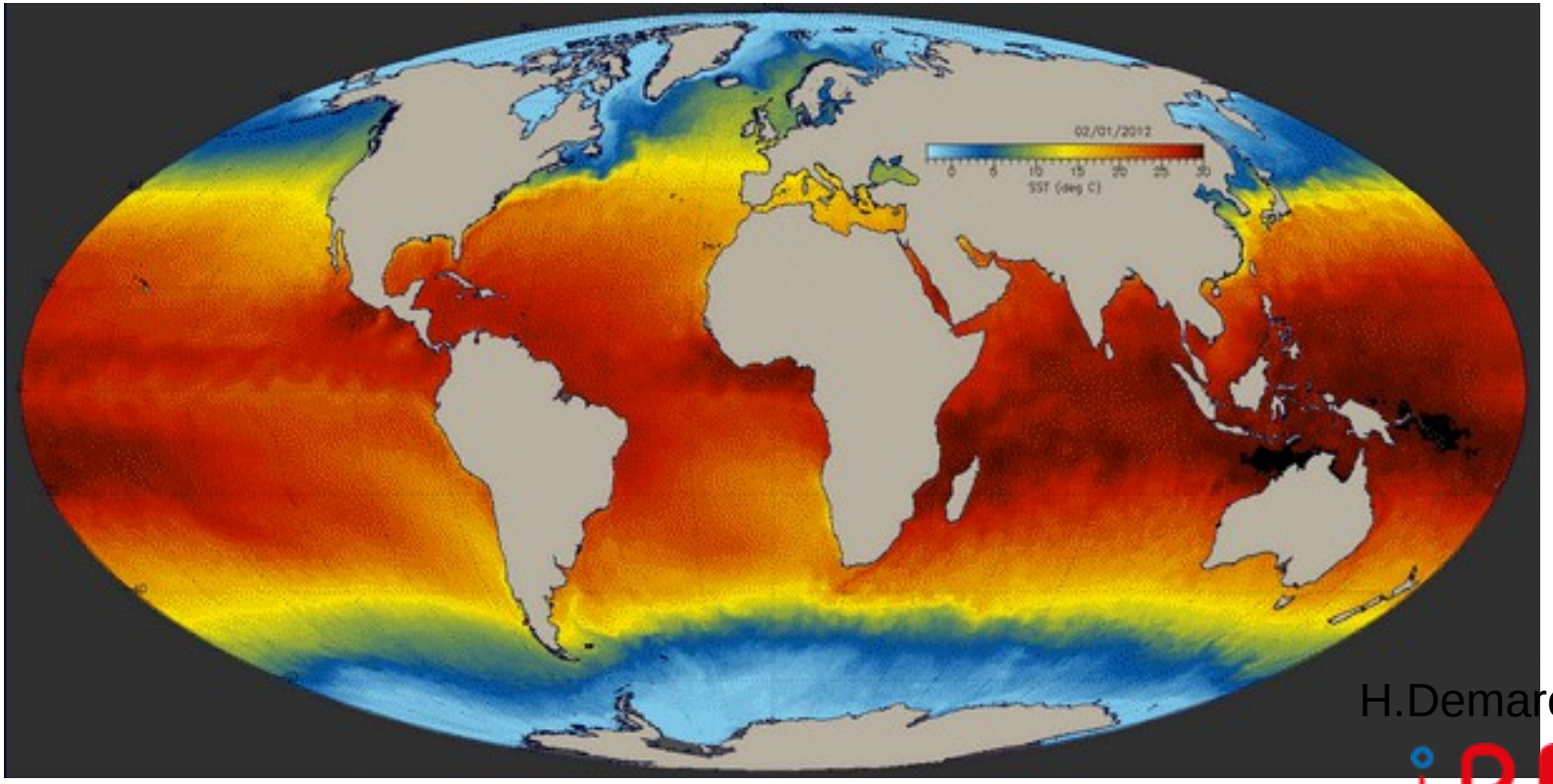

H.Demarcq

Institut de Recherche pour le Développement FRANCE

Ministério da Economia Marítima

OSCM Ocean Science Centre Mindelo

GOBIERNO DE ESPAÑA

Ekman Dynamics

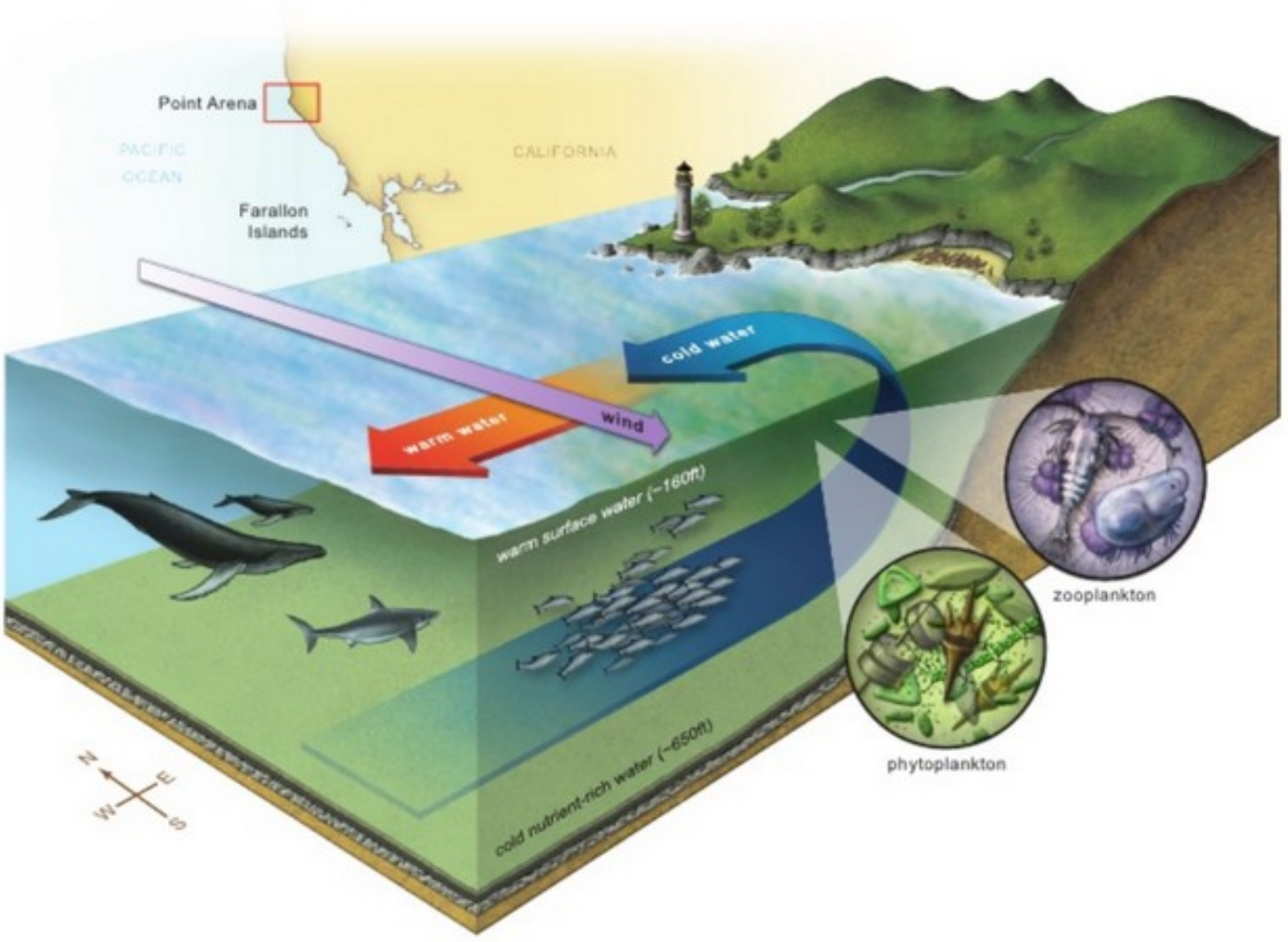
Point Arena
PACIFIC
OCEAN
CALIFORNIA
Farallon
Islands
cold water
warm water
wind
warm surface water (~160ft)
cold nutrient-rich water (~650ft)
zooplankton
phytoplankton
N
E
S
W

Wind Stress

- Wind blowing over the sea surface produces a force per unit area called the **wind stress**.
- The effects of the wind stress are transmitted down into the water column by the action of turbulent eddies generated by breaking waves and boundary shear stresses.

- Let's consider a 2D example, with wind in the x-direction at the ocean surface.
- Horizontal momentum is transferred in the vertical direction.
- For small dz, the stress is proportional to the velocity difference between z+dz and z+dz/2:

$$\tau_{xz} = A_z \frac{\partial u}{\partial z}$$

where A_z is the "eddy viscosity".

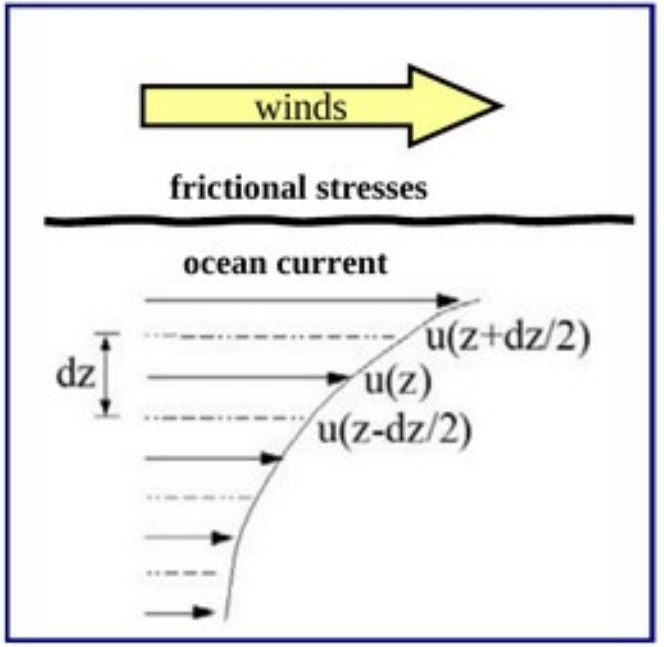

Ekman Layer Thickness

- The Ekman equations are a balance between rotation and friction:

$$-f\ \tilde{v} = A_V \frac{\partial^2 \tilde{u}}{\partial z^2} \qquad (1)$$

$$f(\tilde{u} + U) = A_V \frac{\partial^2 \tilde{v}}{\partial z^2} \qquad (2)$$

Ekman Equations

- Taking: $\frac{\partial^2}{\partial z^2}(1) \Rightarrow (2)$

  we eliminate $\tilde{v}$ and:

$$\frac{D^4 \tilde{u}}{Dz^4} + \frac{f^2}{A_V^2}\tilde{u} = 0$$

- The solution of this equation is given by:

$$\tilde{u} = C_1 e^{(1+i)z/\delta_E} + C_2 e^{(1-i)z/\delta_E} + C_3 e^{-(1+i)z/\delta_E} + C_4 e^{-(1-i)z/\delta_E}$$

where $\delta_E = \sqrt{\frac{A_V}{|f|/2}}$ is the **Ekman layer thickness**

- Note that the Ekman layer doesn't depend on U. It depends only on $f^{-1/2}$ and $A_V^{1/2}$. The idealized turbulent eddy viscosity coefficient A_V, used instead of molecular viscosity, is assumed to be constant with depth although variants on this have been proposed.

Ekman Spiral

- Due to the appearance of the velocity in the y-direction, the velocity vector changes direction within the Ekman layer.
- As each layer of fluid is frictionally retarded by the layer beneath it, the response of the velocity of the upper layer, due to the planetary rotation, is to turn slowly, producing a spiral as z decreases to zero.
- Fig. represents the vectors projected onto the bottom plane. Numbers indicate the relative distance from the plane to the bottom.
- As the bottom approaches, $z \to 0$, and from

$$u = U[1 - e^{-z/\delta_E} \cos(z/\delta_E)]$$
$$v = U e^{-z/\delta_E} \sin(z/\delta_E)$$

it follows:

$$\lim_{z \to 0} \frac{v}{u} = 1$$

- So, the velocity vector has turned 45^0 to the left of the geostrophic vel.

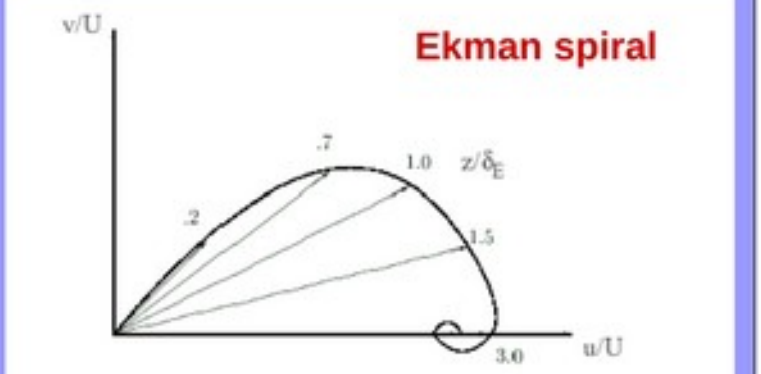

The twist of the velocity vector within the bottom Ekman layer. The deflection is to the left of the current above the layer. (NH)

Ekman Transport

- The mass transport per unity of area in the Ekman layer is calculated by:

$$M_x = \int_0^\infty \tilde{u} dz = -\int_0^\infty U e^{-z/\delta_E} \cos(z/\delta_E) dz = -U\frac{\delta_E}{2}$$

$$M_y = U\frac{\delta_E}{2}$$

$$\Rightarrow \quad \mathbf{M} = \delta_E \frac{U}{2}(-\mathbf{i}+\mathbf{j})$$

- The stress exerted by the rigid surface at z = 0 is:

$$\tau = -\rho A_V \left(\mathbf{i}\frac{\partial u}{\partial z}|_{z=0} + \mathbf{j}\frac{\partial v}{\partial z}|_{z=0} \right) = -\frac{A_V}{\delta_E}\rho U(\mathbf{i}+\mathbf{j}).$$

- Taking the vectorial product between the stress τ and the unit vector in the z-directon:

$$\tau \times \mathbf{k} = \tau_y \mathbf{i} - \tau_x \mathbf{j} = \frac{A_V \rho U}{\delta_E}(-\mathbf{i}+\mathbf{j}).$$

- Multiplying the above term by δ_E / δ_E, we have: $\tau \times \mathbf{k} = \frac{A_V \rho U \delta_E}{2A_V / f}(-\mathbf{i}+\mathbf{j})$

which gives: $\mathbf{M_E} = \frac{\tau \times \mathbf{k}}{\rho f}$

This means that the Ekman transport is 90⁰ to the right of the frictional stress (NH)

Ekman Surface Layer

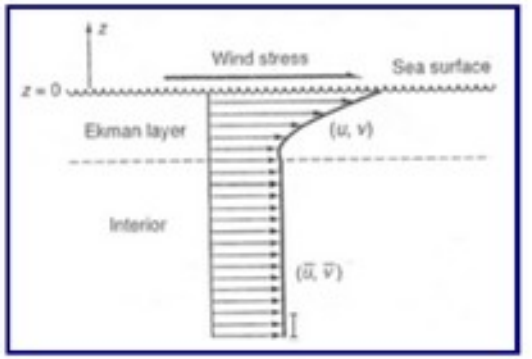

- Using the boundary conditions:
- (1) at the surface (z = 0):

$$\tau_{zx} = -\rho A_V \frac{\partial \tilde{u}}{\partial z}|_{z=0}$$

$$\tau_{zy} = -\rho A_V \frac{\partial \tilde{v}}{\partial z}|_{z=0}$$

- (2) Below the Ekman layer (z→-∞):

$$\tilde{u}(z \to -\infty) \to 0$$

$$\tilde{v}(z \to -\infty) \to 0$$

- Then $A_2 = A_4 = 0$ and $A_3 = i\,A_1$, with

$$A_1 = \frac{\tau_{zx}\delta_E}{2\rho A_V}\left(\frac{1-i}{2}\right)$$

- So, substituting the constants back to the solution, we have:

$$\tilde{u}(z) = \frac{\tau_{zx}\delta_E}{\sqrt{2}\rho A_V} e^{z/\delta_E} \sin\left(\frac{z}{\delta_E} + \frac{\pi}{4}\right)$$

$$\tilde{v}(z) = -\frac{\tau_{zx}\delta_E}{\sqrt{2}\rho A_V} e^{z/\delta_E} \sin\left(\frac{z}{\delta_E} + \frac{\pi}{4}\right)$$

So, at the surface

$$\tilde{u}(z=0) = \frac{\sqrt{2}}{2} V_0$$

$$\tilde{v}(z=0) = -\frac{\sqrt{2}}{2} V_0$$

surface current at 45⁰ to the right (NH)

where $V_0 = \sqrt{u^2|_{z=0} + v^2|_{z=0}} = \frac{\tau_{zx}\delta_E}{\sqrt{2}\rho A_V} = \frac{\tau_{zx}}{\rho\sqrt{f A_V}}$

Ekman Transport

- Similarly to the Ekman bottom layer, we can also calculate the integrated transport in the surface layer:

$$\mathbf{M} = \frac{\tau \times \mathbf{k}}{\rho f}$$

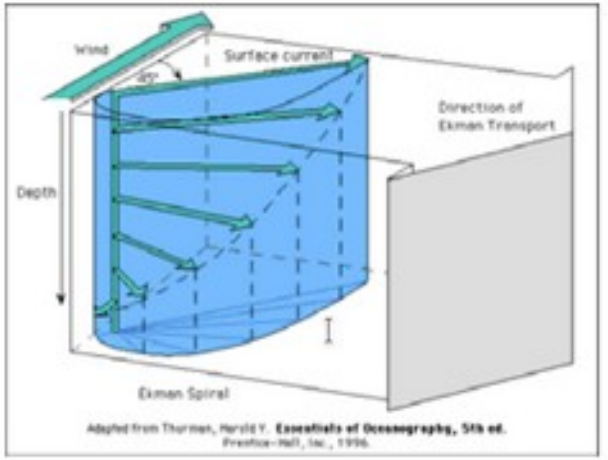

Ekman transport is 90^0 to the right of the wind stress in the Northern Hemisphere left of the wind stress in the Southern Hemisphere

Questions:

- Given a typical eddy viscosity coefficient is of order 10^{-2} m^2 s^{-1}, and f is ~ 10^{-4} s^{-1},

1. Then what is the order of magnitude of Ekman layer?
2. How strong is the surface current produced by a wind stress of 0.1Pa?

$$\delta_E = \sqrt{\frac{A_V}{|f|/2}}$$

$$V_0 = \frac{\tau_{zx}}{\rho\sqrt{fA_V}}$$

Ekman Summary (so far)

Surface Current:

45⁰ to the right (left) in the NH (SH)

Ekman layer detph: $\delta_E = \sqrt{\frac{A_V}{|f|/2}}$

$$\tilde{u}(z=0) = \frac{\sqrt{2}}{2} V_0$$

$$\tilde{v}(z=0) = -\frac{\sqrt{2}}{2} V_0$$

$$V_0 = \frac{\tau_{zx}}{\rho\sqrt{fA_V}}$$

Ekman transport:

90⁰ to the right (left) in the NH (SH)

$$\mathbf{M} = \frac{\tau \times \mathbf{k}}{\rho f}$$

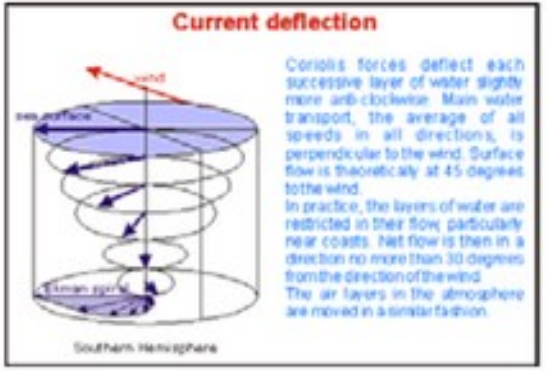

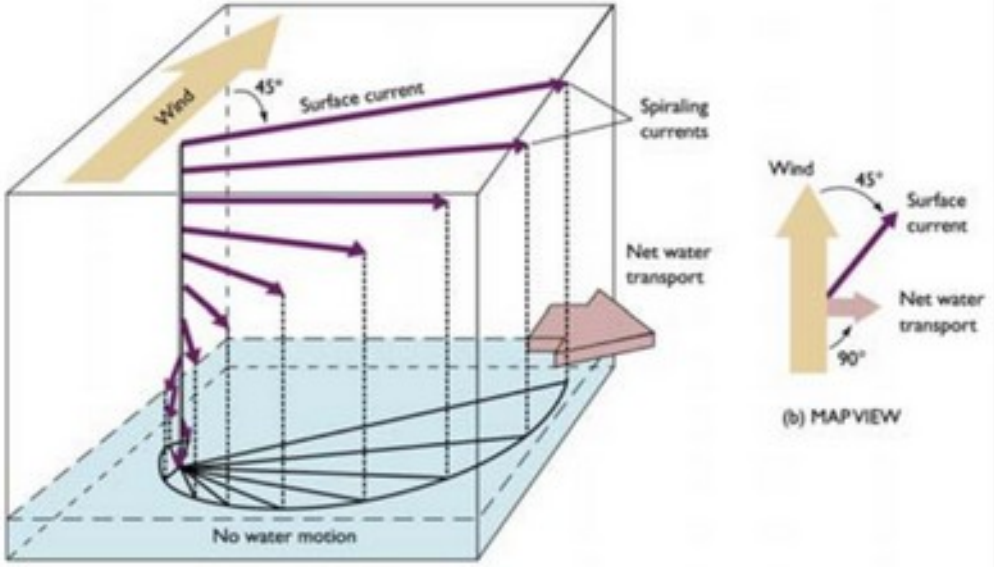

Global Wind Pattern

In the globe we have 3 major wind systems in each hemisphere: Polar easterlies, mid-latitude westerlies and the trade winds (easterlies)

- Look at the direction of the winds below and answer what happens to the Ekman transport?

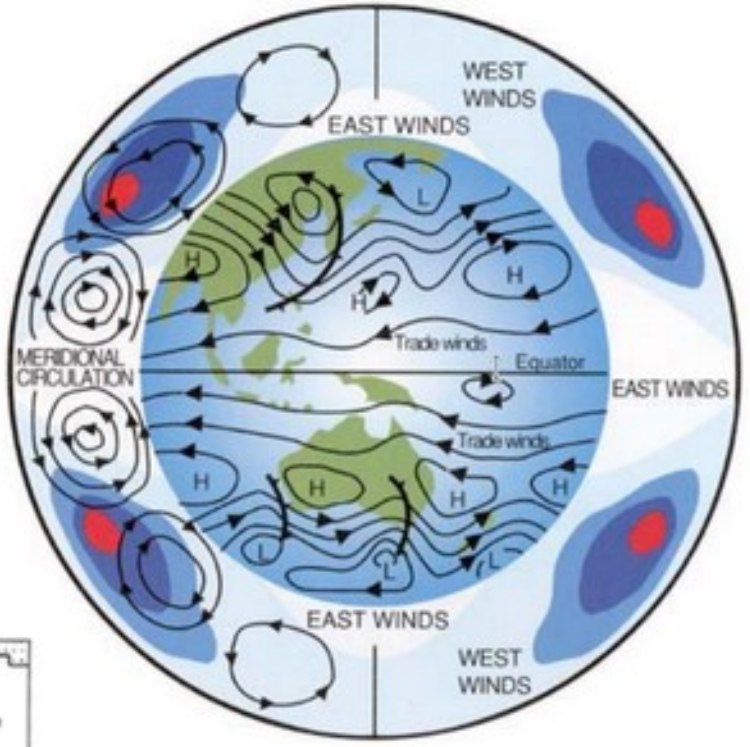

- What happen to this convergence (divergence)?

Ekman Pumping

- Integrating the continuity equation from the bottom to the top of the Ekman surface layer, we have:

$$\frac{\partial M_x}{\partial x} + \frac{\partial M_y}{\partial y} = w_0 - w_E$$

where w_0 is the vertical velocity at the ocean surface and w_E is the vertical velocity at the bottom of the Ekman layer.

- But w_0 is negligible compared to w_E. Using the relations between M and τ, we define the **Ekman pumping velocity**:

$$w_E = \mathbf{k} \cdot \nabla \times \frac{\tau}{f}$$

- This is a very important property of Ekman dynamics because it allow us to know what happen with a flow that convergences or divergence in the ocean.
- This relation says that a **clockwise** wind pattern (**negative curl**) in the **N**orthern **H**emisphere generates **downwelling**, whereas a **counterclockwise** wind pattern causes **upwelling**. The directions are opposite in the Southern Hemisphere.

Ekman Pumping

- Consider the stress field in the x-direction, but varying in intensity in the y-direction.
- The Ekman transport is to the right of the applied wind stress.

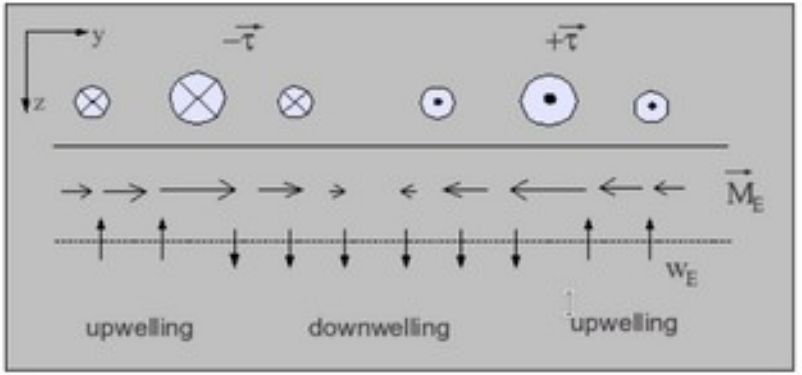

- Because the wind stress intensity is varying, the transport also varies and causes convergence and divergence in certain regions.
- To conserve mass, fluid is sucked into the Ekman layer at a rate proportional to the divergence of the Ekman flux ($w_E > 0$).
- The inverse occurs in the convergence regions.
- So, there is a net movement of water away from equator. As a consequence, there is a positive Ekman pumping that causes upwelling in the equator.

Ekman Pumping

- In the subtropics, where midlatitude westerlies and the trades coalesce, the net transport generates convergence (subtropical gyres). It generates an upward bulge in the sea surface (and a downward depression of the thermocline).
- These bulges are very slight, i.e. changes of order O(1m) over distances of 100's of km.

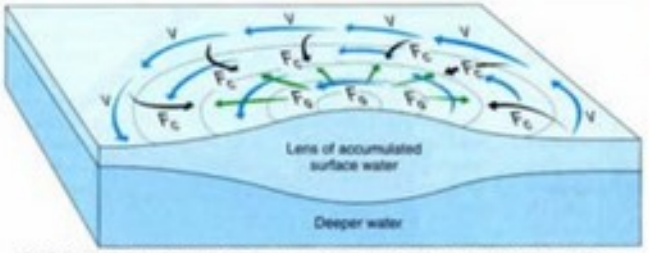

Fig.5 Currents flow (V) around a gyre when the inward Ekman transport due to the Coriolis effect (Fc) is balanced by Fg, the outward force due to gravity.

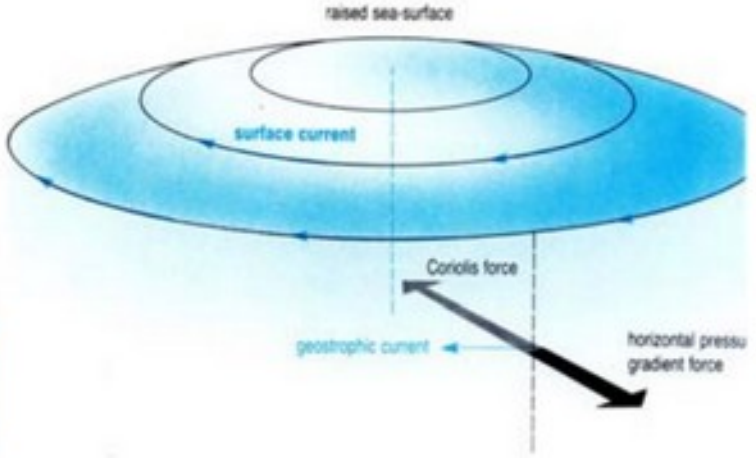

The generation of geostrophic current flow in a gyre driven by anticyclonic winds in the Northern Hemisphere. This current is driven by the wind only indirectly and persists below the wind-drive (Ekman) layer.

AGU100 ADVANCING EARTH AND SPACE SCIENCE

JGR

Journal of Geophysical Research: Oceans

RESEARCH ARTICLE

10.1029/2018JC014187

Key Points:

- New upwelling indices are presented for the U.S. West Coast (31–47°N) to address shortcomings in historical indices
- The Coastal Upwelling Transport Index (CUTI) estimates vertical volume transport (i.e., upwelling/downwelling)
- The Biologically Effective Upwelling Transport Index (BEUTI) estimates vertical nitrate flux

Supporting Information:

- Supporting Information S1

Correspondence to:
M. G. Jacox,
michael.jacox@noaa.gov

Citation:
Jacox, M. G., Edwards, C. A., Hazen, E. L., & Bograd, S. J. (2018). Coastal upwelling revisited: Ekman, Bakun, and improved upwelling indices for the U.S. West Coast. *Journal of Geophysical Research: Oceans, 123*. https://doi.org/10.1029/2018JC014187

Coastal Upwelling Revisited: Ekman, Bakun, and Improved Upwelling Indices for the U.S. West Coast

Michael G. Jacox[1,2], Christopher A. Edwards[3], Elliott L. Hazen[1], and Steven J. Bograd[1]

[1]NOAA Southwest Fisheries Science Center, Monterey, CA, USA, [2]NOAA Earth System Research Laboratory, Boulder, CO, USA, [3]University of California, Santa Cruz, CA, USA

Abstract Coastal upwelling is responsible for thriving marine ecosystems and fisheries that are disproportionately productive relative to their surface area, particularly in the world's major eastern boundary upwelling systems. Along oceanic eastern boundaries, equatorward wind stress and the Earth's rotation combine to drive a near-surface layer of water offshore, a process called *Ekman transport*. Similarly, positive wind stress curl drives divergence in the surface Ekman layer and consequently upwelling from below, a process known as *Ekman suction*. In both cases, displaced water is replaced by upwelling of relatively nutrient-rich water from below, which stimulates the growth of microscopic phytoplankton that form the base of the marine food web. Ekman theory is foundational and underlies the calculation of upwelling indices such as the "Bakun Index" that are ubiquitous in eastern boundary upwelling system studies. While generally valuable first-order descriptions, these indices and their underlying theory provide an incomplete picture of coastal upwelling. Here we review the relevant dynamics and limitations of classical upwelling indices, particularly related to representation of the surface wind stress, the influence of geostrophic currents, and the properties of upwelled water. To address these shortcomings, we present two new upwelling indices for the U.S. West Coast (31–47°N), which are available from 1988 to present. The Coastal Upwelling Transport Index and the Biologically Effective Upwelling Transport Index provide improved estimates of vertical transport and vertical nitrate flux, respectively, by leveraging technological and scientific advances realized since the introduction of the Bakun Index nearly a half century ago.

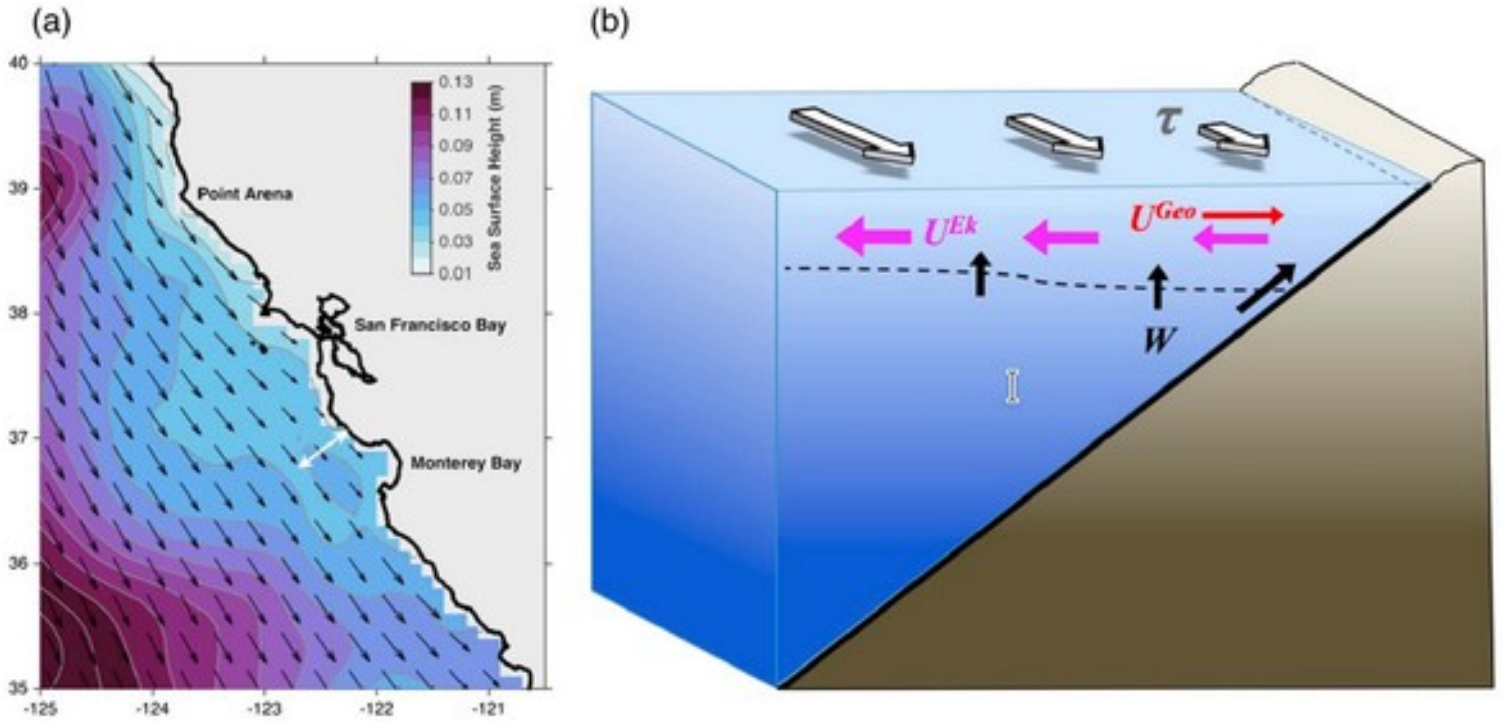

Figure 1. (a) Mean 1988–2017 sea surface height (in color) and wind stress (arrows) during the upwelling season (March–August) off the central/northern California coast, obtained from the California Current System Regional Ocean Modeling System reanalyses; (b) schematic representation of a coastal section corresponding to the white line in (a), showing key components of the upwelling dynamics of central importance to this paper: Alongshore wind stress (τ), an alongshore sea surface height gradient, Ekman transport ($\boldsymbol{U}^{\boldsymbol{Ek}}$), geostrophic transport ($\boldsymbol{U}^{\boldsymbol{Geo}}$), vertical transport ($W$), and the depth of the surface mixed layer (dashed line).

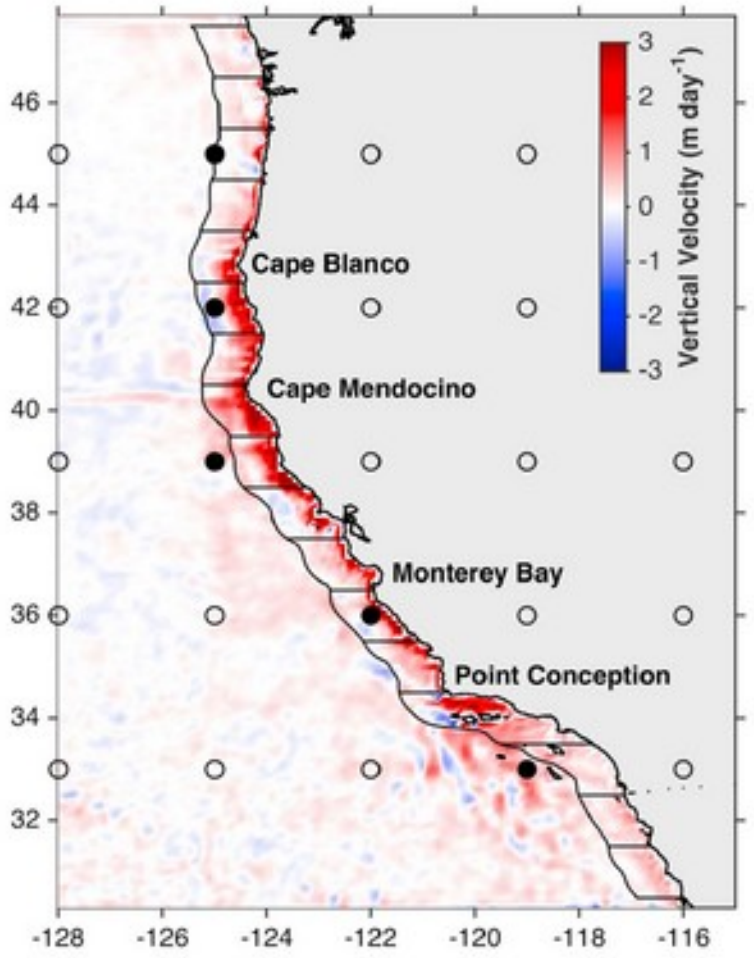

Figure 2. Mean 1988–2017 vertical velocity at the base of the mixed layer during the upwelling season (March–August), obtained from the Regional Ocean Modeling System reanalyses. The 3° Fleet Numerical Meteorology and Oceanography Center sea level pressure grid is overlaid, with filled circles indicating locations used historically for calculation of the Bakun Index. Black lines outline regions of integration for the new upwelling indices.

shelves, with sustained upwelling favorable winds, and in regions of strong stratification (Barton et al., 1977; Estrade et al., 2008; Jacox & Edwards, 2011; Lentz & Chapman, 2004). Similarly, curl-driven upwelling can be important very close to shore, particularly in the lee of capes and headlands where expansion fans in the marine boundary later occur within tens of kilometers of the coast (Dever et al., 2006; Fiechter et al., 2014; Koračin & Dorman, 2001; Pickett & Paduan, 2003). Furthermore, wind products with higher spatial resolution show the coastal wind drop-off occurring in a narrower coastal band (Capet et al., 2004), increasing the overlap of estimated upwelling due to coastal divergence and wind stress curl. Thus, while upwelling variability near shore is out of phase with upwelling variability farther offshore (Jacox et al., 2014), neither can be attributed solely to coastal divergence or wind stress curl.

3. Revisiting the Bakun Index

The Bakun Index methodology was originally laid out in two technical reports (Bakun, 1973, 1975) that while highly cited are challenging to obtain. A more accessible report by Schwing et al. (1996) also details the Bakun Index calculation, and we review it here. While some of the details of the Bakun Index calculation have changed over time, the methodology has not. Here we present the original calculation described by Bakun (1973) and implemented by NOAA. After this overview we describe changes employed in subsequent iterations of the index.

An estimate of sea level pressure (SLP) is obtained from an operational atmospheric model run by the U.S. Navy's Fleet Numerical Meteorology and Oceanography Center (FNMOC), formerly the Fleet Numerical Weather Center. SLP gradients are then estimated at the grid points corresponding to upwelling index locations (Figure 2) by calculating the pressure difference between grid points on either side and dividing by the distance between them. Because the initial FNMOC grid resolution

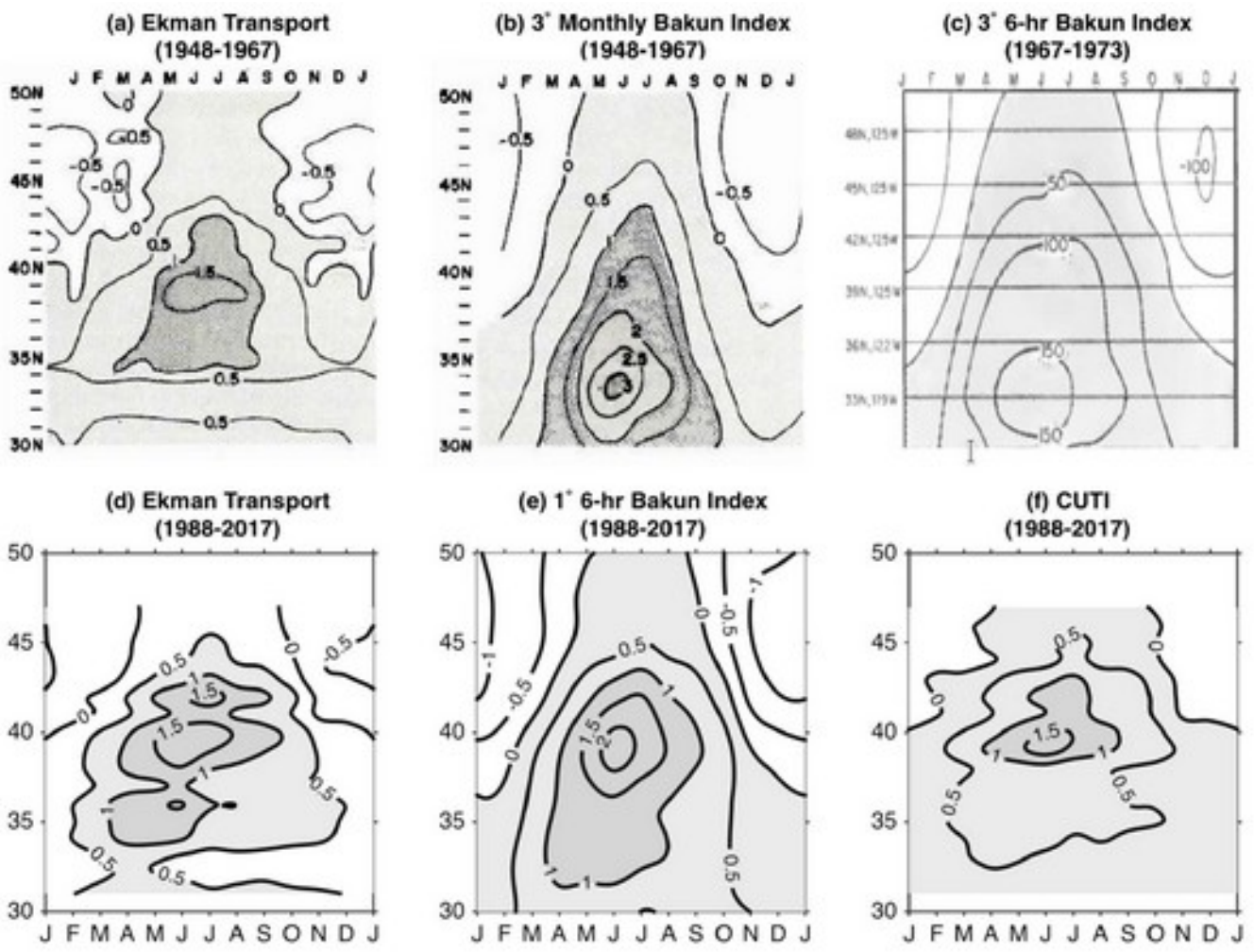

Figure 3. Climatological transport estimates are plotted against latitude for (top) transport indices as described by Bakun (1973, 1975): (a) Ekman transport estimated from in situ wind measurements (adapted from Bakun, 1973), (b) Bakun Index calculated from monthly 3° sea level pressure (SLP) fields (adapted from Bakun, 1973), (c) Bakun Index calculated from 6-hourly 3° SLP fields (adapted from Bakun, 1975) and (bottom) transport indices calculated 1988–2017: (d) Ekman transport estimated from California Current System Regional Ocean Modeling System reanalysis winds, (e) Bakun Index calculated from 6-hourly 1° SLP fields, (f) revised upwelling index (Coastal Upwelling Transport Index) described herein. Note that panel (c) uses units of m^3/s per 100-m coastline, so values are a factor of 100 greater than in the other panels, which use units of m^3/s per meter coastline (i.e., m^2/s).

"The 1° 6-hr index is best of the three for the post-1996 period when FNMOC has provided SLP fields at 1° resolution"

In addition to uncertainties in the Ekman transport calculation, the Bakun Index does not (and does not try to) capture several important contributors to upwelling dynamics. First is wind stress curl-driven upwelling associated with alongshore wind gradients (i.e., $d\tau_0{}^x/dy$ for a coastline oriented in the y-direction), though the Bakun Index does inherently include wind stress curl-driven upwelling associated with zonal gradients in the alongshore wind stress (i.e., $d\tau_0{}^y/dx$) inshore of the location where the index is calculated. Second is the contribution of the cross-shore geostrophic flow. If the constraint of no horizontal pressure gradient is removed from Ekman theory, equation (1) for the zonal velocity becomes

$$fu = \frac{1}{\rho}\frac{\partial \tau^y}{\partial z} - g\frac{\partial \eta}{\partial y} \tag{6}$$

and equation (2) becomes

$$U^{Ek} + U^{geo} = \frac{\tau_0^y}{\rho f} - \frac{gD}{f}\frac{\partial \eta}{\partial y} \tag{7}$$

where η is the free surface height, g is the gravitational acceleration, and U^{geo} is the zonal geostrophic trans-

4. Improved Upwelling Indices

- The Coastal Upwelling Transport Index (CUTI, pronounced “cutie”), which is comparable to the Bakun Index in that it is an estimate of the total volume of water upwelled or downwelled in a given time period (i.e., the vertical volume flux into or out of the surface layer).

- Second is the Biologically Effective Upwelling Transport Index (BEUTI, pronounced “beauty”), which is an estimate of the total quantity of nitrate upwelled or downwelled in a given time period (i.e., the vertical nitrate flux into or out of the surface layer). BEUTI therefore quantifies not only the intensity of upwelling but also the quality of upwelled waters in terms of their nutrient content, which can strongly influence productivity independent of the surface wind strength (Jacox, Bograd, et al., 2015; Jacox et al., 2016).

Note: here, the ocean state estimates and surface wind forcing are obtained from historical reanalyses of the CCS produced using the Regional Ocean Modeling System (ROMS) with 4-dimensional variational data assimilation.

This method accounts for Ekman transport associated with alongshore wind stress as well as wind stress curl in both the alongshore and cross-shore directions. In contrast, Ekman transport estimated from alongshore wind stress at some offshore location (as in the Bakun Index) omits Ekman suction/pumping associated with alongshore wind stress gradients.

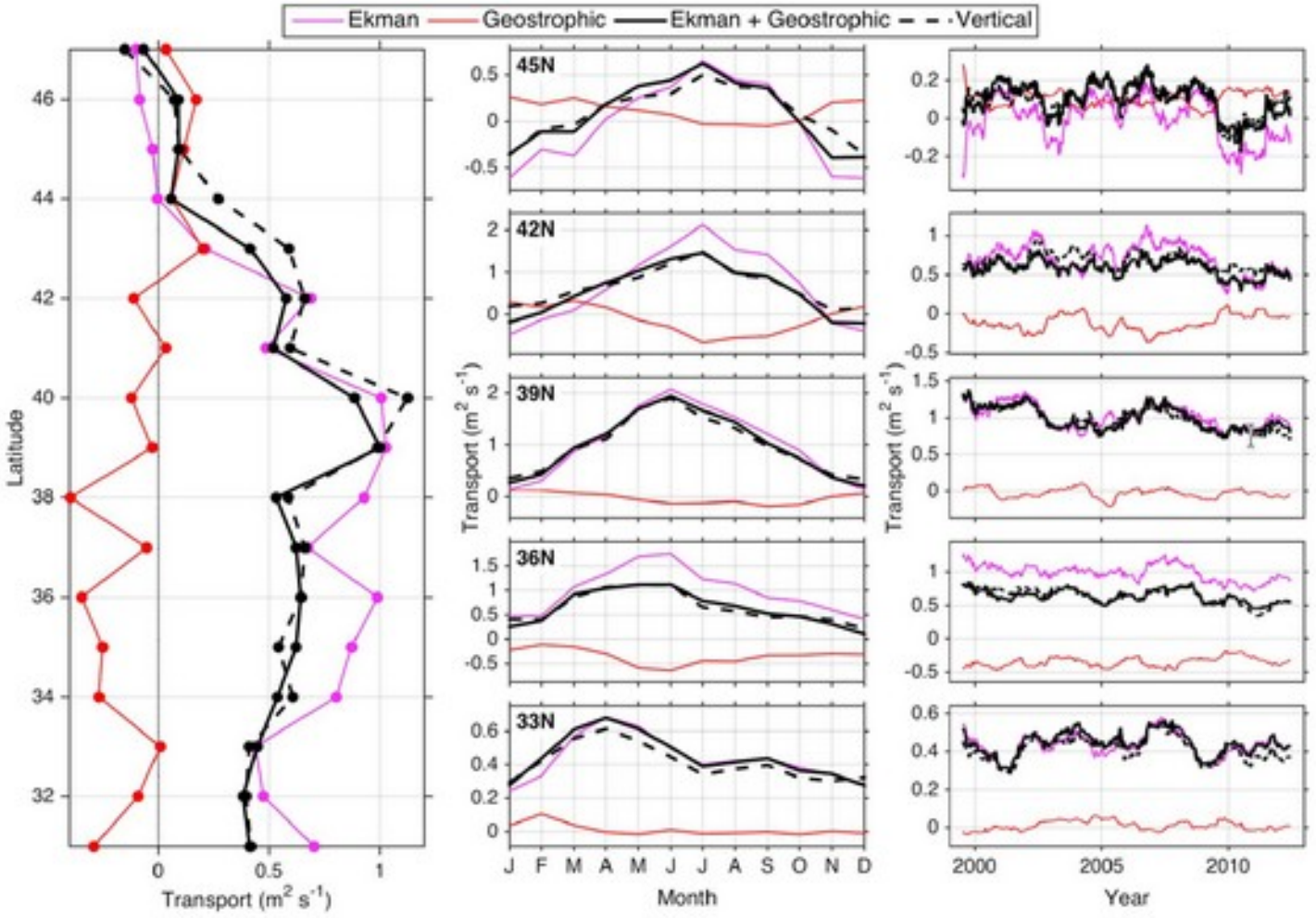

Figure 4. (left) Long-term mean, (middle) seasonal climatology, and (right) interannual variability of transport components, plotted against latitude (left panel) or at select latitudes (middle and right panels). Positive values are upwelling favorable. Transport components were calculated from CCSRA14 for 1999–2012 (see sections 4.1 and 4.2). Interannual variability was calculated by smoothing daily time series with a 12-month running mean. The temporal coverage of the new indices is longer (1988 to present), but they are constructed from multiple reanalyses. Here we focus on a single self-consistent reanalysis to explore individual terms in the transport budget. Note scale differences on *y*-axes of middle and right panels.

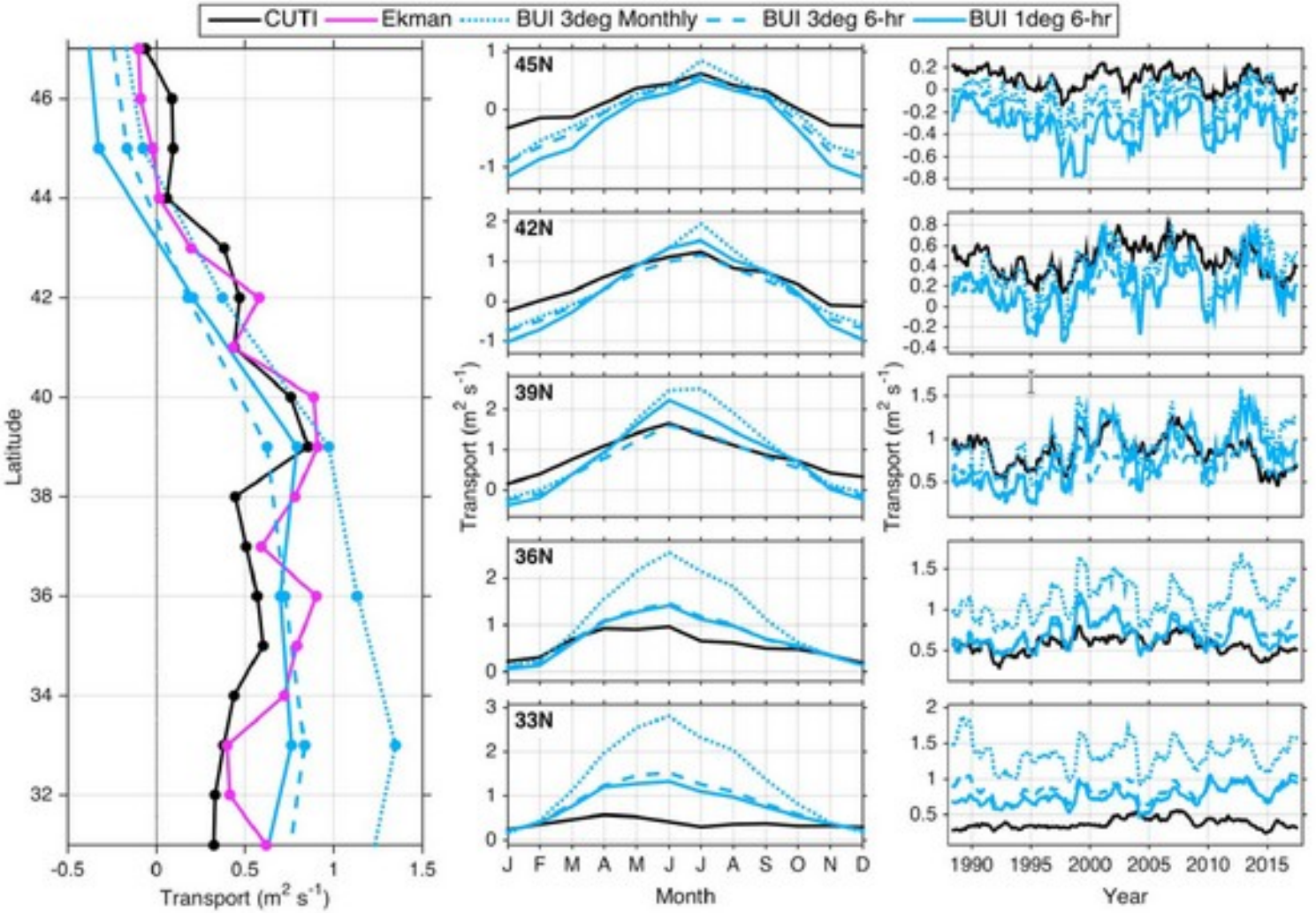

Figure 8. (left) Long-term mean, (middle) seasonal climatology, and (right) interannual variability (12-month running mean) of CUTI and multiple versions of the Bakun Index (BUI), plotted against latitude (left panel) or at select latitudes (middle and right panels). The long-term mean Ekman transport component of CUTI is also plotted for comparison. Indices are shown for 1988–2017. Note scale differences on y-axes of middle and right panels. CUTI = Coastal Upwelling Transport Index.

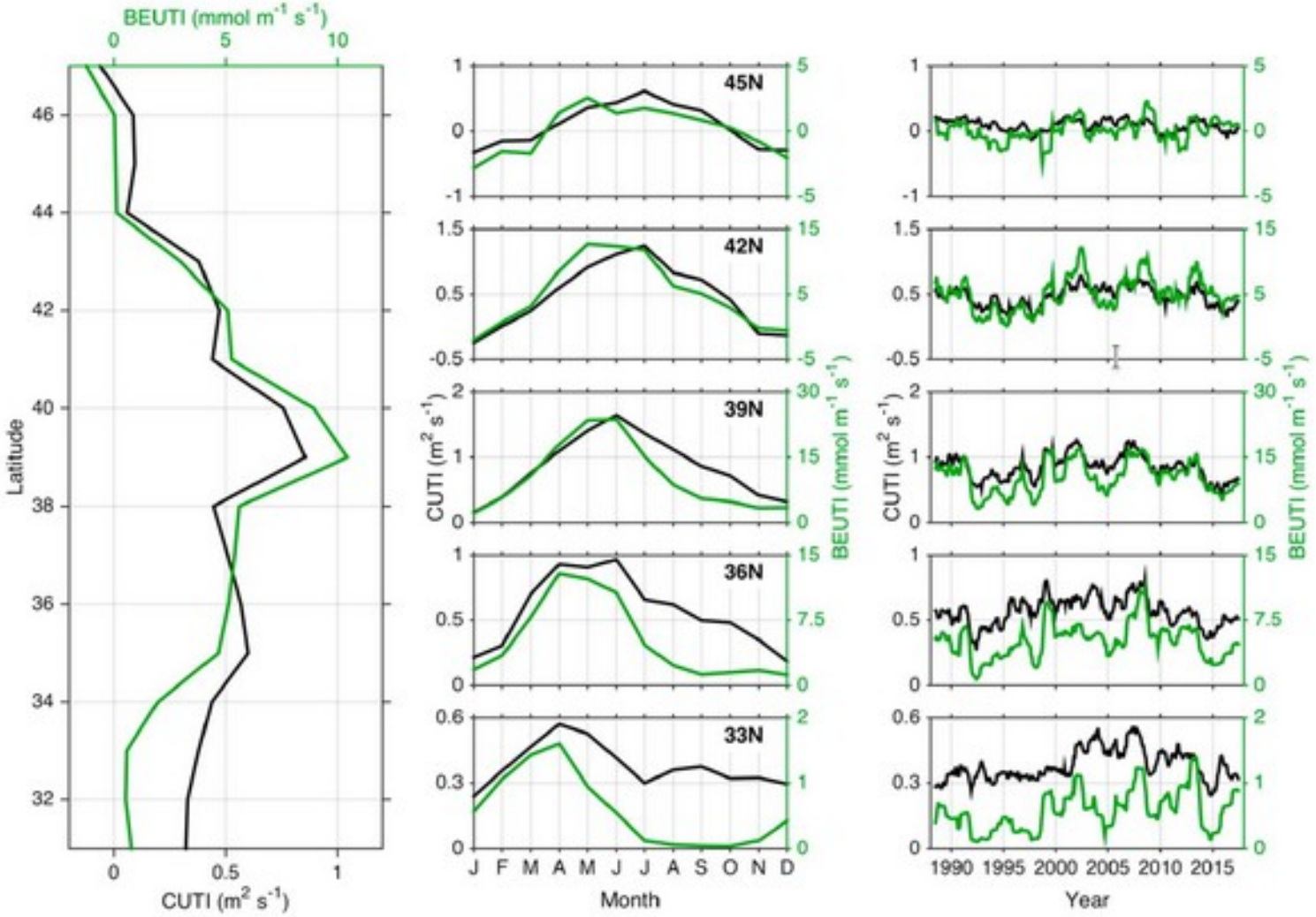

Figure 10. (left) Long-term mean, (middle) seasonal climatology, and (right) interannual variability (12-month running mean) of CUTI and BEUTI, plotted against latitude (left panel) or at select latitudes (middle and right panels). Indices are shown for 1988–2017. Note scale differences on *y*-axes of middle and right panels. CUTI = Coastal Upwelling Transport Index; BEUTI = Biologically Effective Upwelling Transport Index.

7.2. Creating Similar Indices for Other Regions

A key strength of the Bakun Index is that in theory it can be calculated for any coastline in the global ocean. In regions where the oceanographic model output needed to calculate CUTI or BEUTI are unavailable, SLP (or better yet surface wind stress) from atmospheric reanalyses can be used to estimate upwelling. We suggest calculating Ekman transport as we have here, by integrating along all boundaries of the region of interest rather than rotating winds and estimating offshore transport. Integration around the region of interest eliminates the need for estimating the coastline orientation, ensures that Ekman transport/pumping associated with alongshore and cross-shore variations in the wind are captured, and enables more accurate closure of the transport budget. In regions where high-resolution oceanographic analyses are available, the methodology presented here can be applied to create similar indices.

➡ We must see together what is the best to compute it for the Canary System

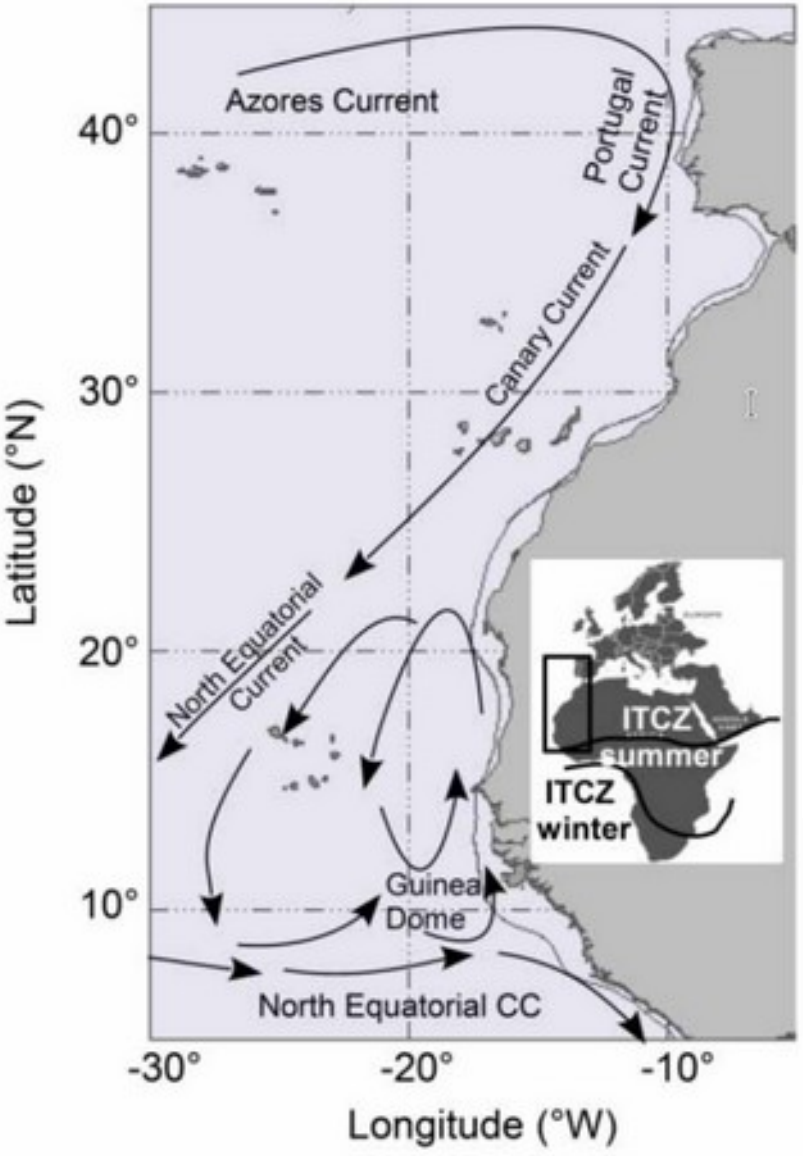

6.3. RECENT CHANGES AND TRENDS OF THE UPWELLING INTENSITY IN THE CANARY CURRENT LARGE MARINE ECOSYSTEM

Aïssa BENAZZOUZ[1], Hervé DEMARCQ[2] and Gonzalo GONZÁLEZ-NUEVO[3]

[1] Institut National de Recherche Halieutique. Morocco

[2] Institut de Recherche pour le Développement. France

[3] Centro Oceanográfico de Vigo, Instituto Español de Oceanografía. Spain

6.3.2. DATASETS

We use two homogeneous datasets from spatial observation: a 30 years SST series from the AVHRR (Advanced Very High Resolution Radiometer) version 5.2 day-time for the time period September 1981 to December 2011 (http://www.nodc.noaa.gov/sog/pathfinder at 4 km resolution, accessed on 15 October 2014), and the global wind CCMP (Cross-Calibrated Multi-Platform) from July 1987 until 2010 funded under the United States National Aeronautics and Space Administration (NASA) Earth Science Enterprise (Atlas et al., 2010).

The Mean Annual Cycle in Global Ocean Wind Stress

KEVIN E. TRENBERTH, WILLIAM G. LARGE AND JERRY G. OLSON
National Center for Atmospheric Research, Boulder, Colorado*

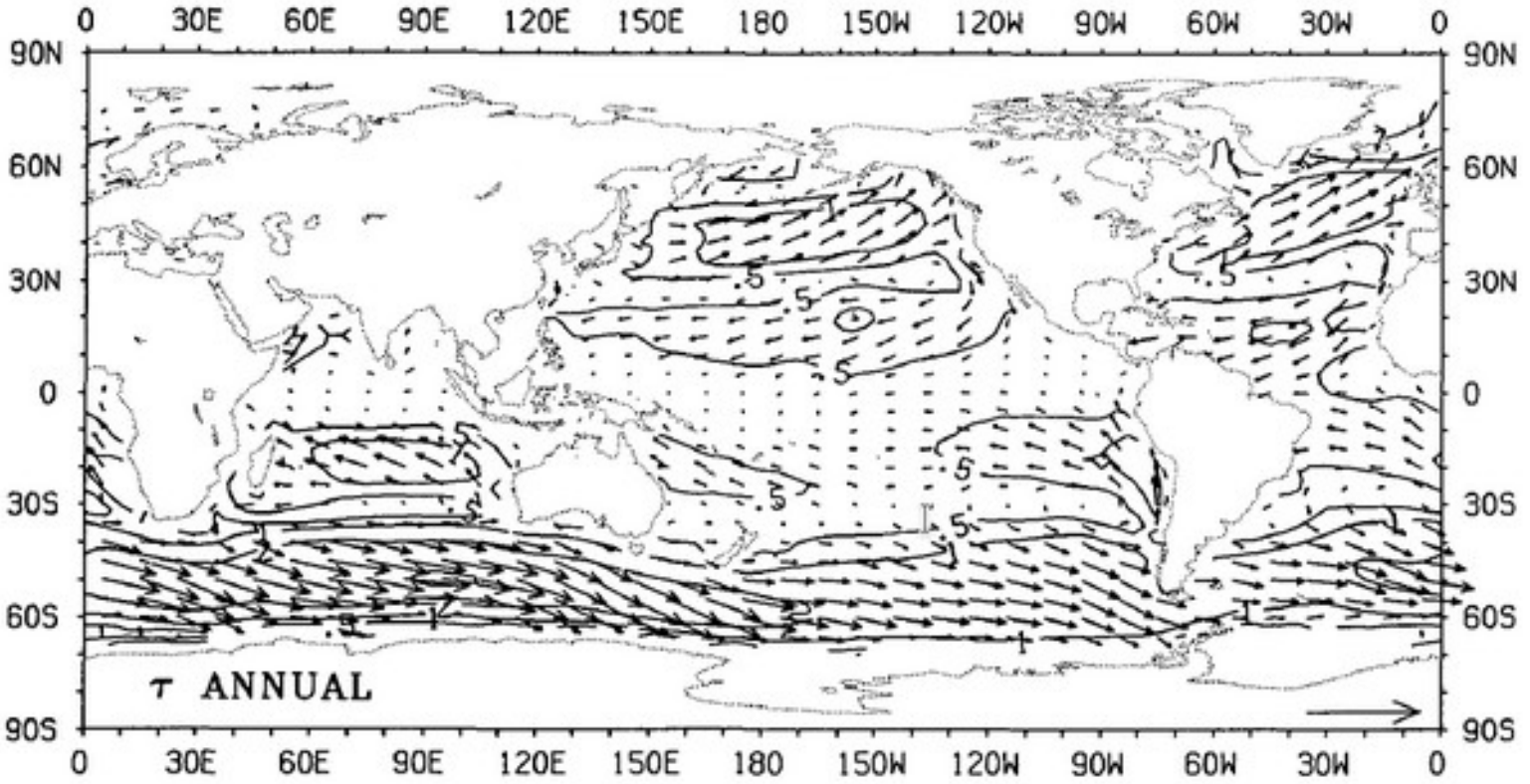

FIG. 1. Annual mean wind stress over the global oceans depicted as vectors. The arrow at bottom right corresponds to 5 dyn cm^{-2} and contours of magnitude of 0.5, 1, 2 and 3 dyn cm^{-2} are plotted.

Wind stress formulation: $$\tau = (\tau_x, \tau_y) = \rho C_D V(u, v) \qquad (1)$$

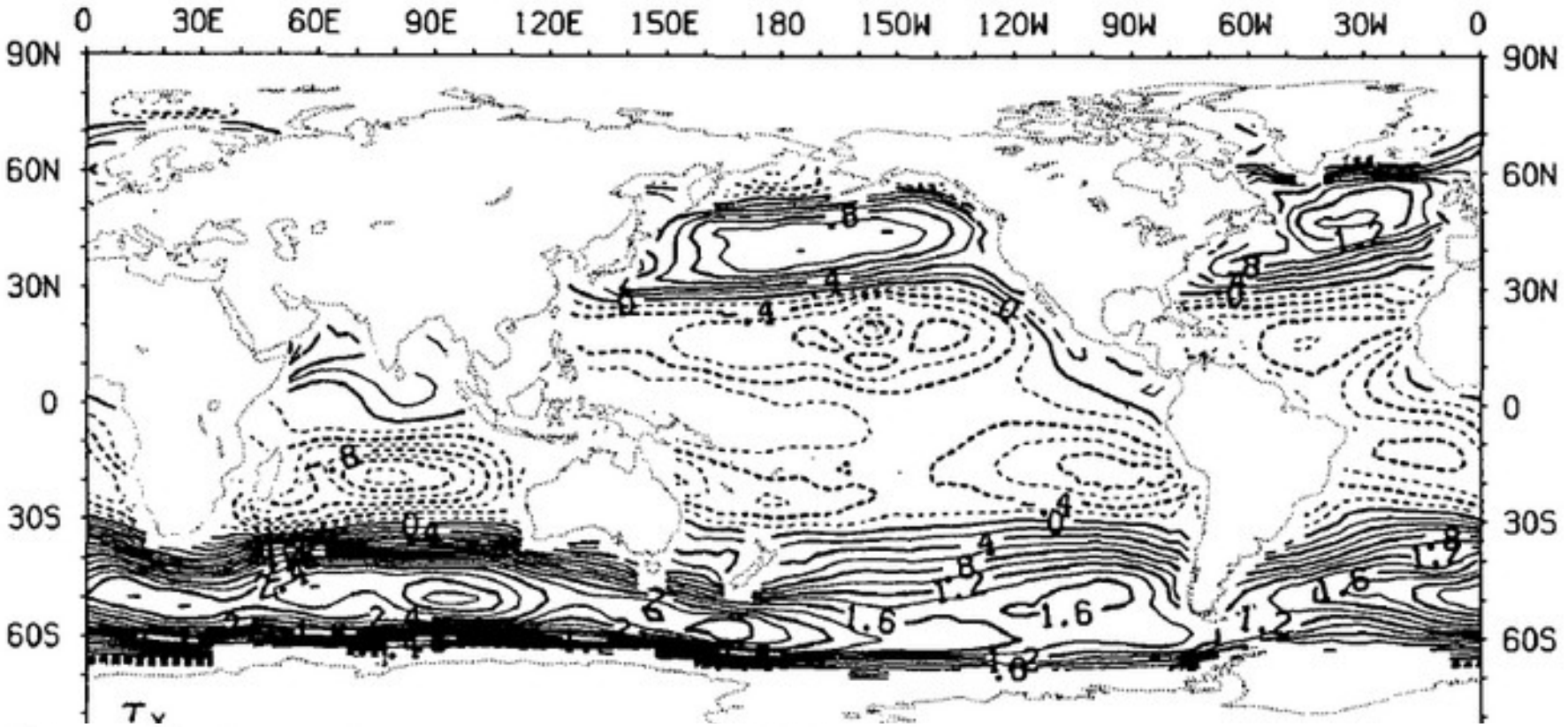

FIG. 2. Annual mean wind stress over the global oceans for the two components. The contour interval is 0.2 dyn cm^{-2}. Negative (westward or southward) values are dashed.

Sydeman et al (2014) : a metadata analysis based on the results of 22 studies from the published litterature.

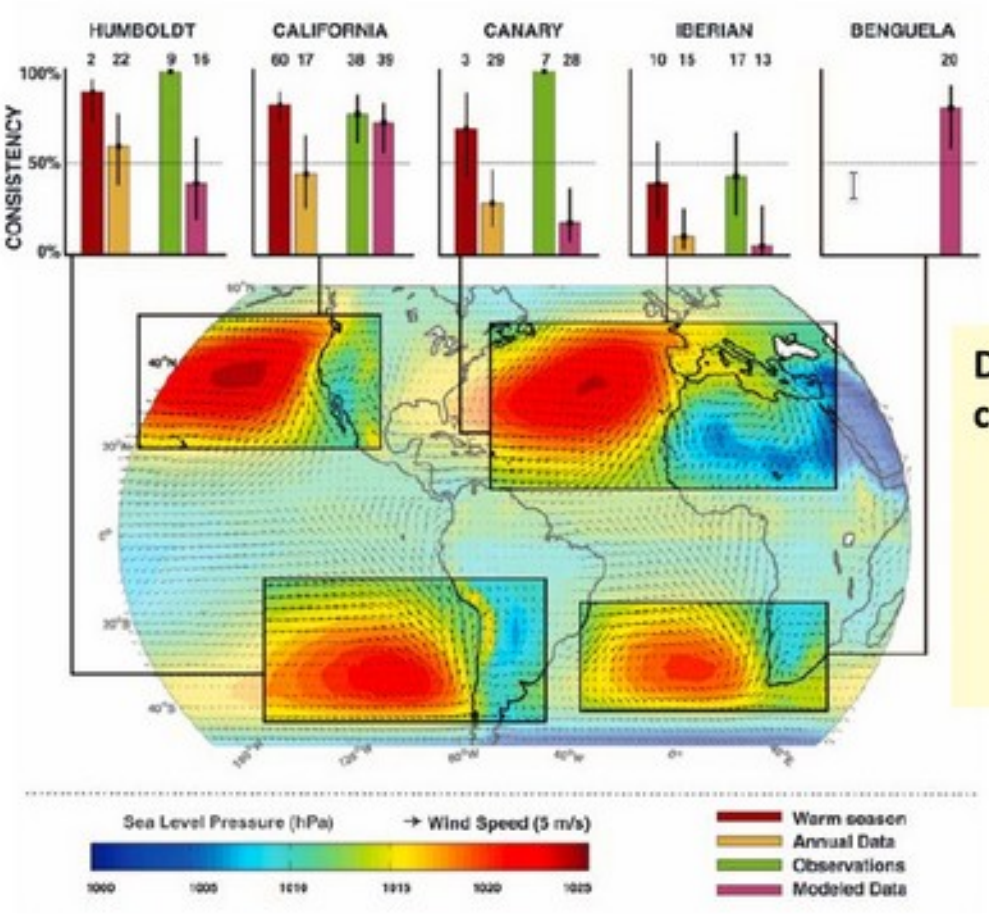

Fig. 1. EBCSs of the world showing warm-season spatial climatologies of sea-level pressure and surface wind fields based on the NCEP/NCAR (National Centers for Environmental Protection/National Center for Atmospheric Research) model-data reanalysis product. These are estimates from logistic regression of consistency with the wind intensification hypothesis; bars show the estimated probability (± 95% confidence intervals). Numbers above the bars denote the number of trends contributing to each point estimate and confidence interval. The dashed horizontal line denotes the null hypothesis of equal probability of increasing or decreasing winds.

Sydeman, W. J., M. Garcia-Reyes, D. S. Schoeman, R. R. Rykaczewski, S. A. Thompson, B. A. Black, and S. J. Bograd (2014), Climate change and wind intensification in coastal upwelling ecosystems, Science, 345(6192), 77-80.

Details on the 198 time-series that were considered by *Sydeman et al. 2014 (SM)* :

- **-80 based on NCEP/NCAR reanalysis**
- **-46 based on ship reports and COADS**
- **-28 based on pressure derived indices**
- **-23 based on data from buoys**

…

Composite CCMP wind (several satellite sources, 1988-2019)

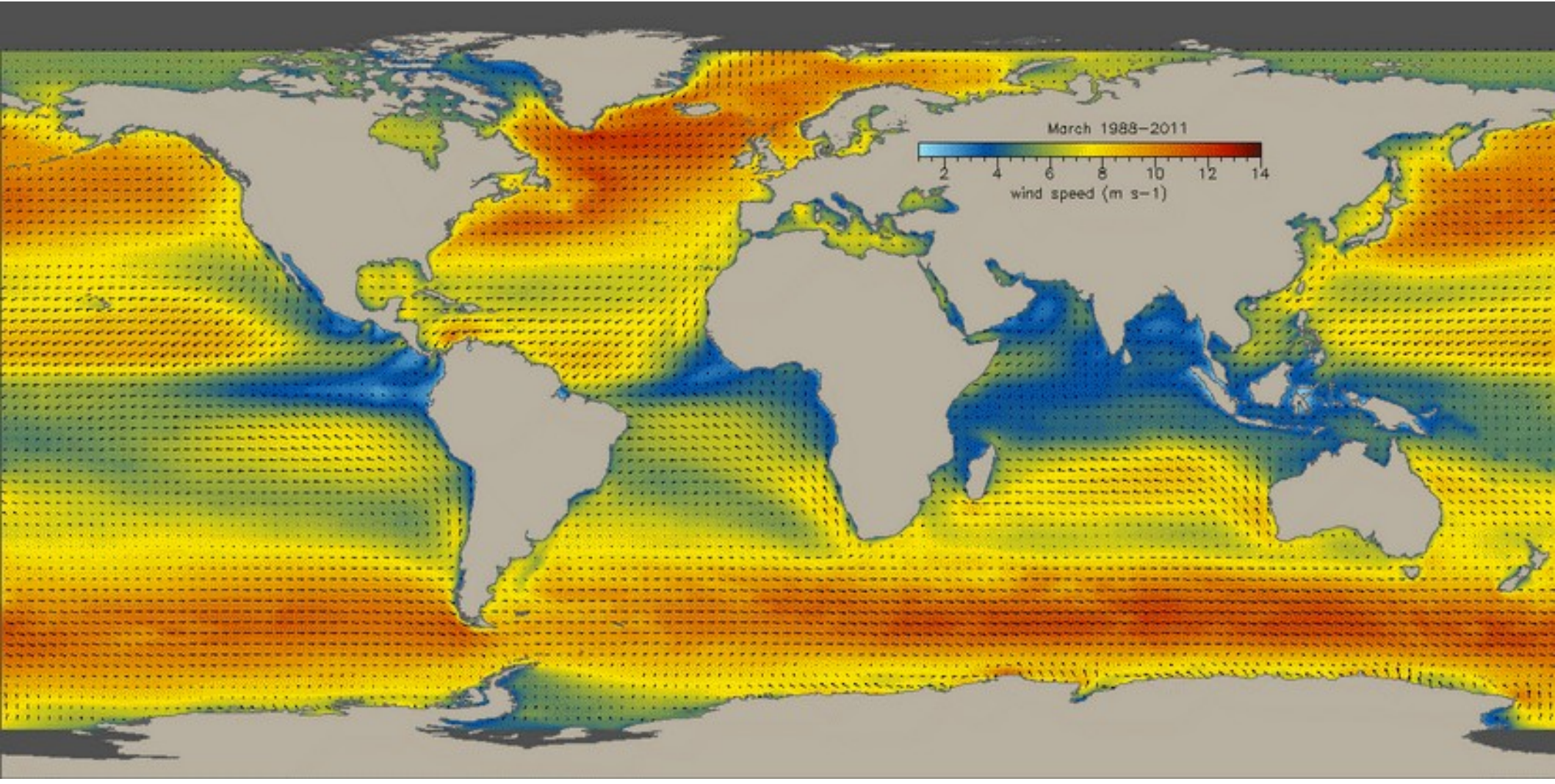

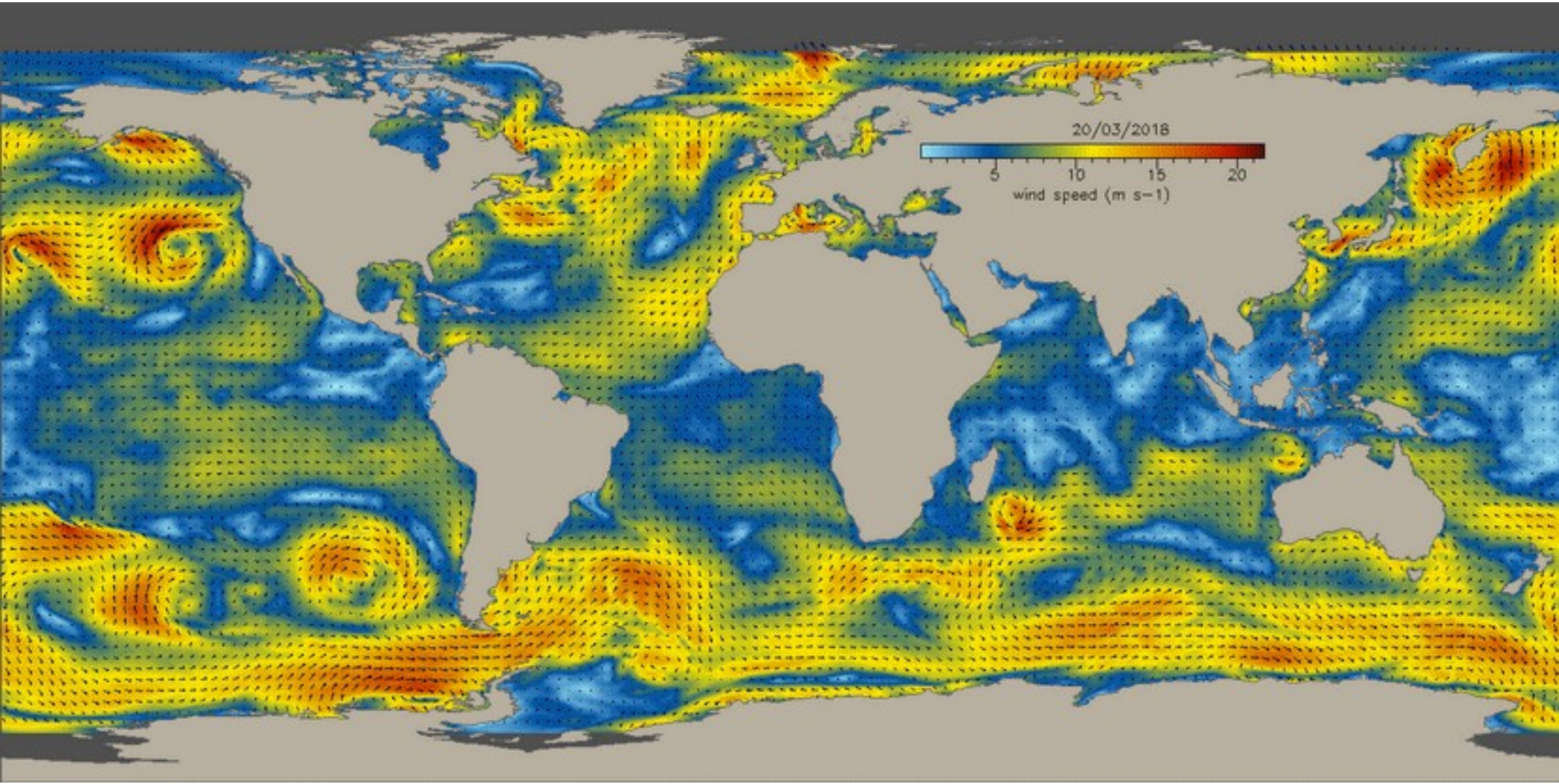
20/03/2018
5
10
15
20
wind speed (m s−1)

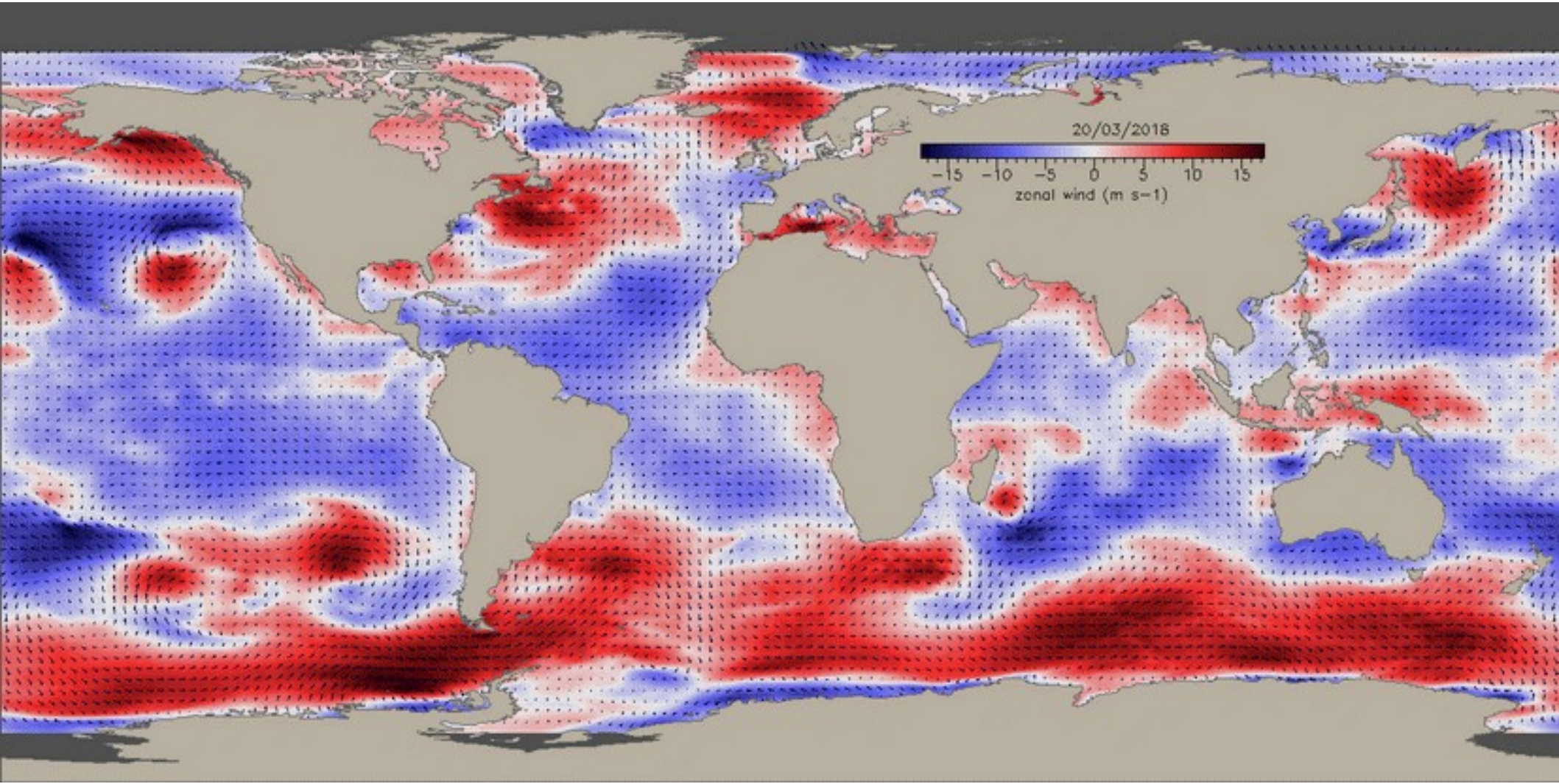
20/03/2018
−15 −10 −5 0 5 10 15
zonal wind (m s−1)

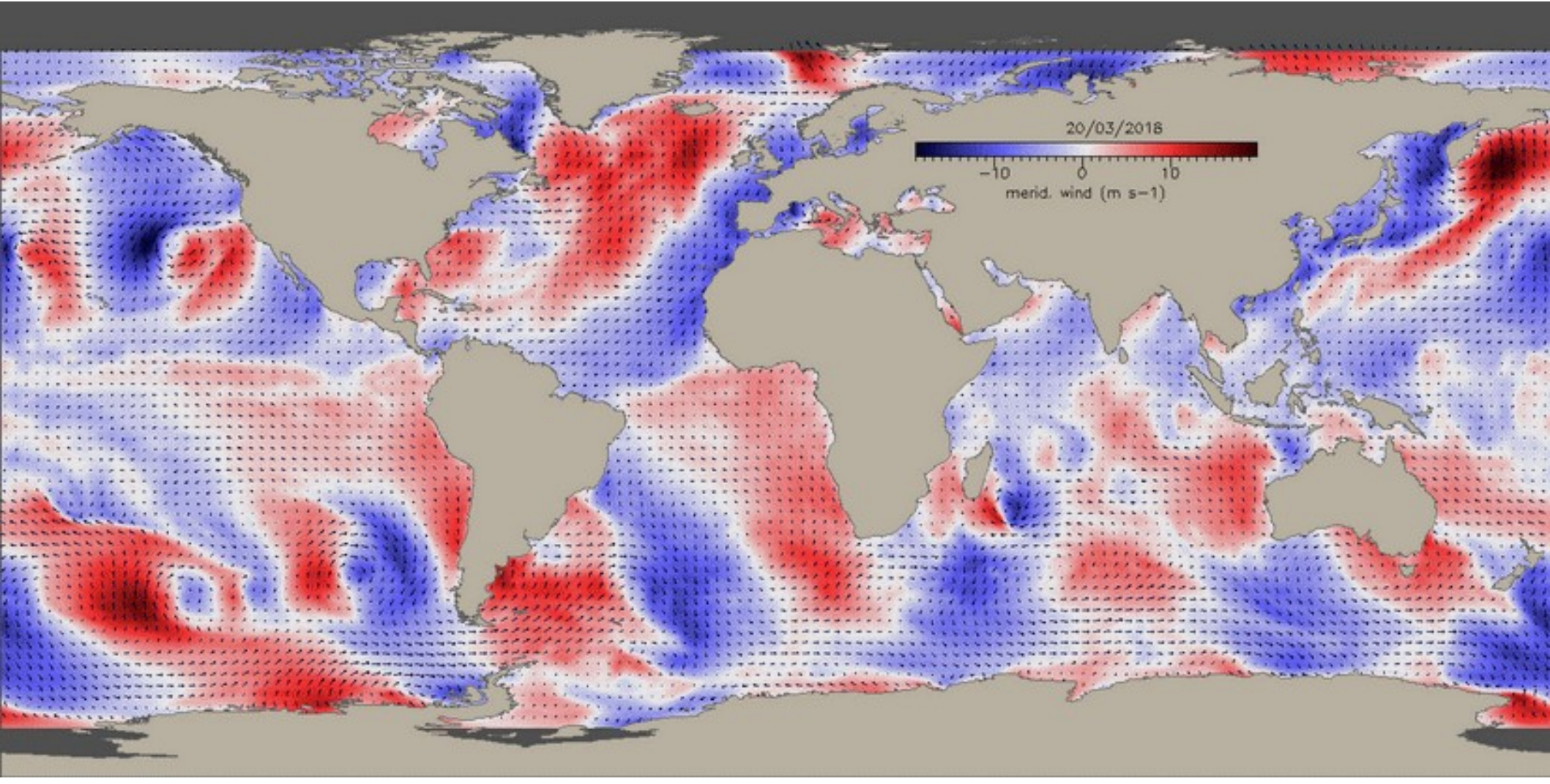
20/03/2018
−10
0
10
merid. wind (m s−1)

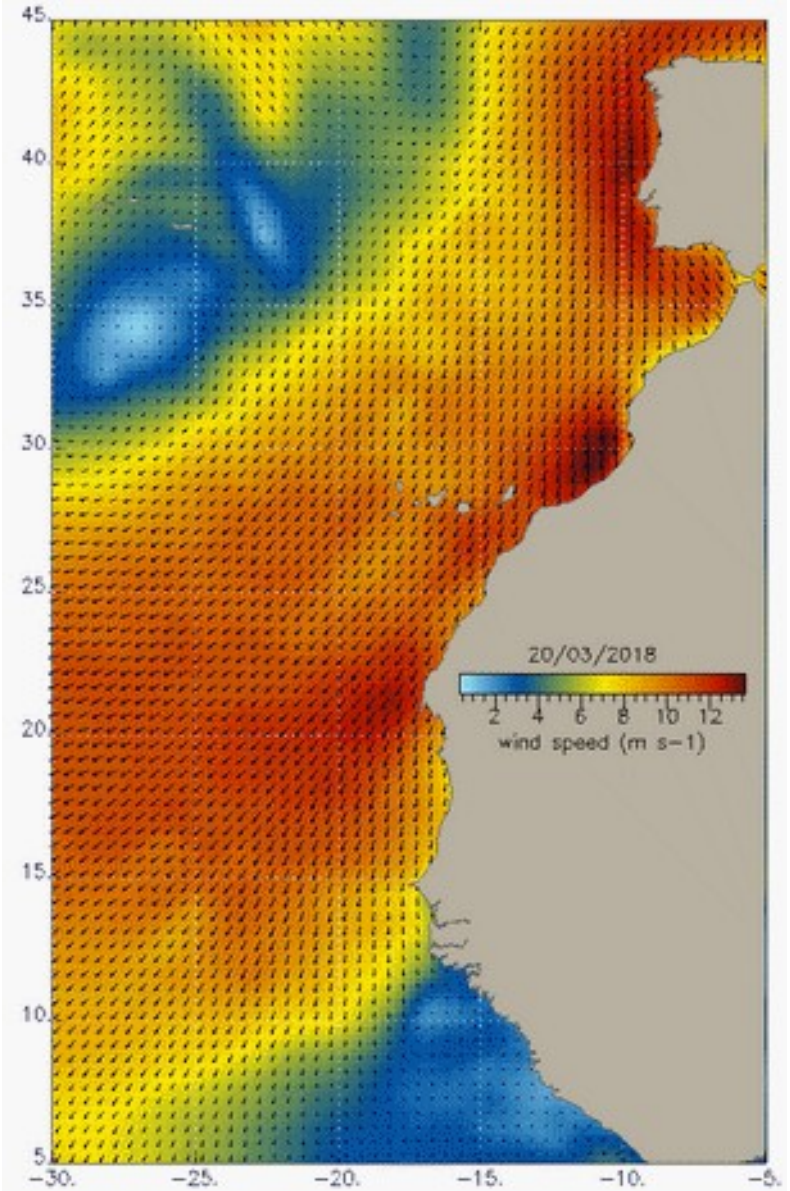
45
40
35
30
25
20
15
10
5
−30.
−25.
−20.
−15.
−10.
−5.
20/03/2018
2 4 6 8 10 12
wind speed (m s−1)

Wind seasonnality (CCMP) from monthly averages (2008)

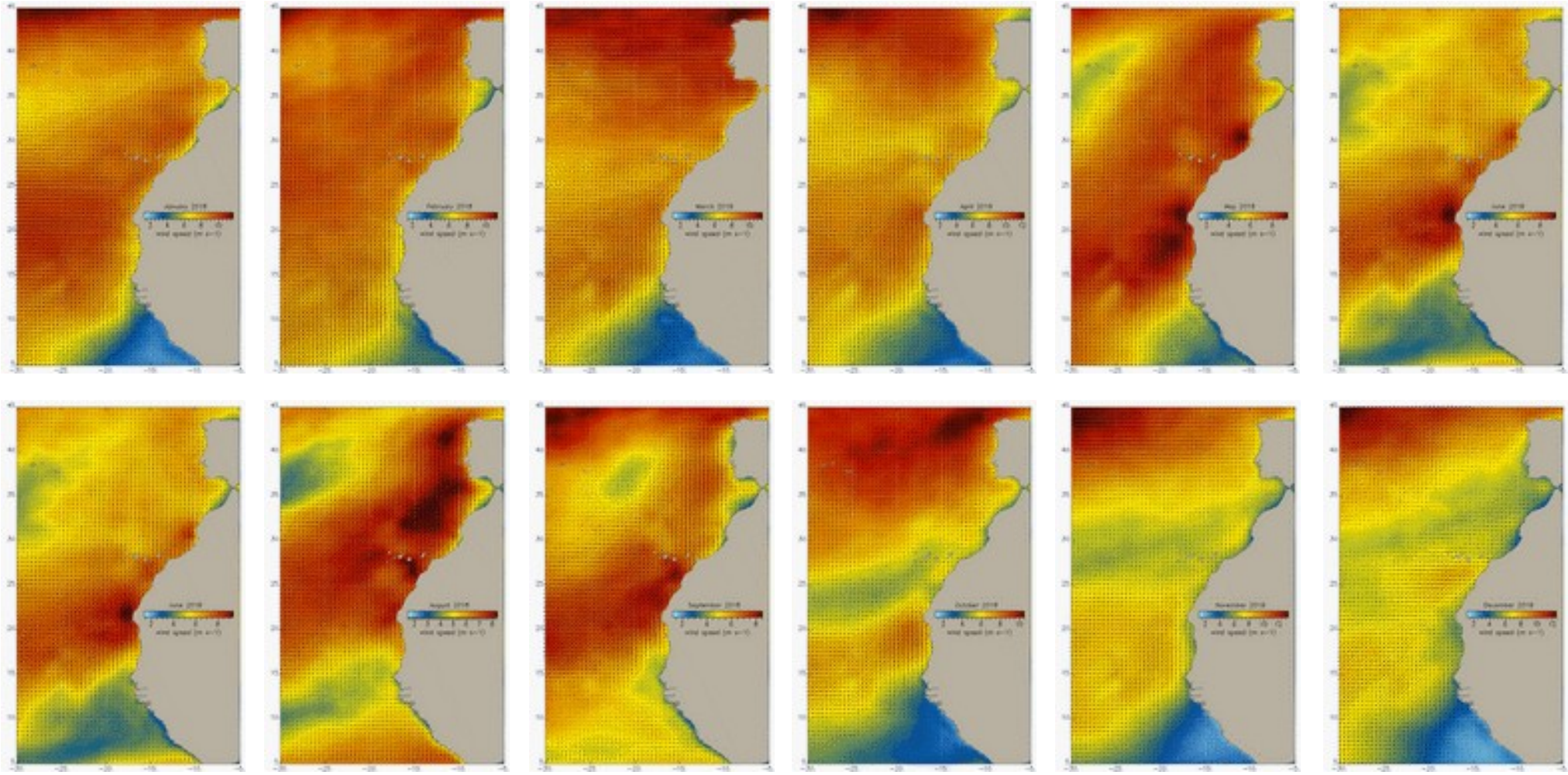

Climatological wind seasonnality (CCMP) from monthly averages

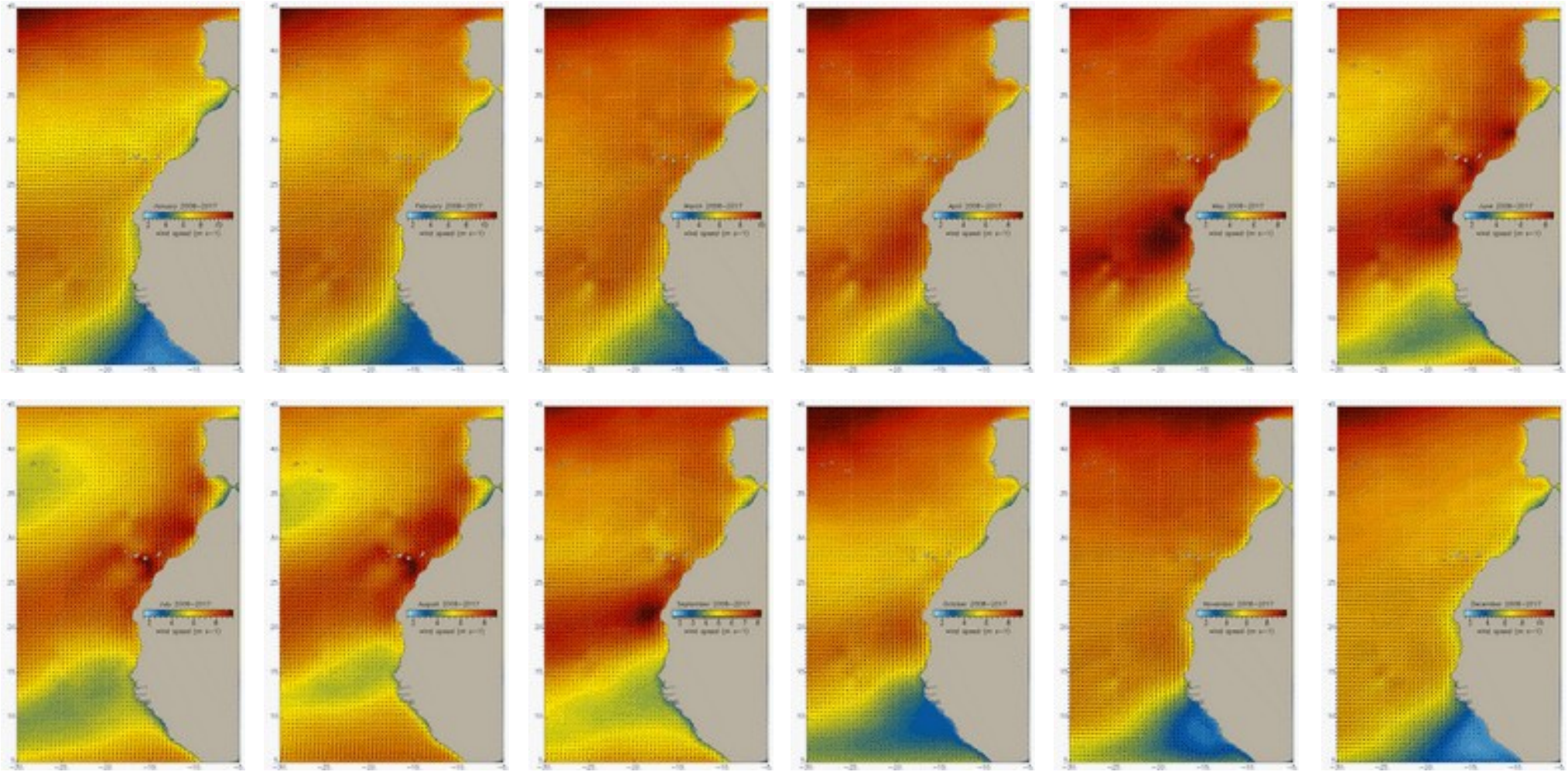

Computation of the wind-based Ekman upwelling index

Contents lists available at ScienceDirect

Continental Shelf Research

journal homepage: www.elsevier.com/locate/csr

Research papers

An improved coastal upwelling index from sea surface temperature using satellite-based approach – The case of the Canary Current upwelling system

Aïssa Benazzouz [a,b,*], Soumia Mordane [a], Abdellatif Orbi [b], Mohamed Chagdali [a], Karim Hilmi [b], Abderrahman Atillah [c], Josep Lluís Pelegrí [d], Hervé Demarcq [e,**]

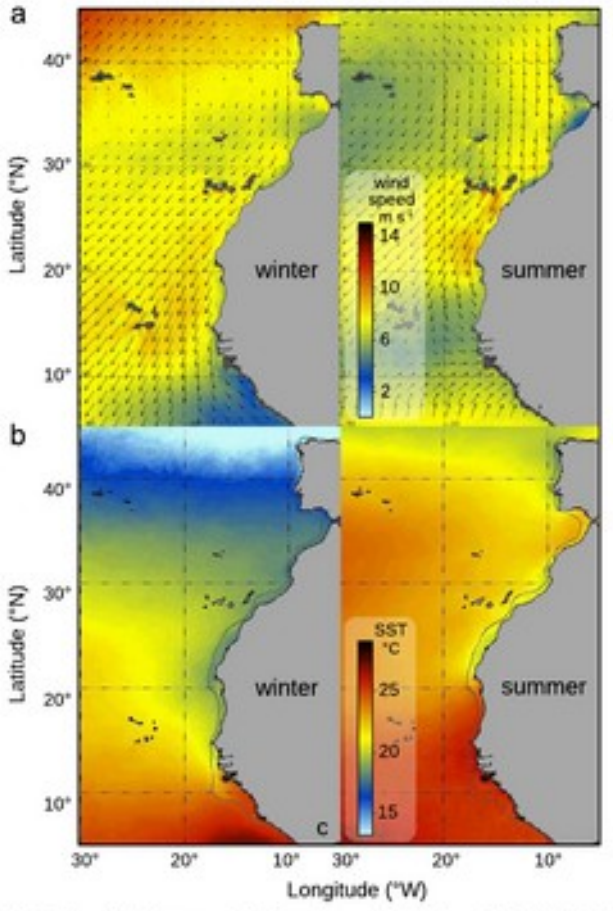

Fig. 2. Climatological means of (a) the surface wind field from QuikSCAT (1999–2009), (b) the SST from AVHRR (1982–2011) in winter (week 02–09 February) and summer (week 04–11 July), with the 200 m isobath superimposed.

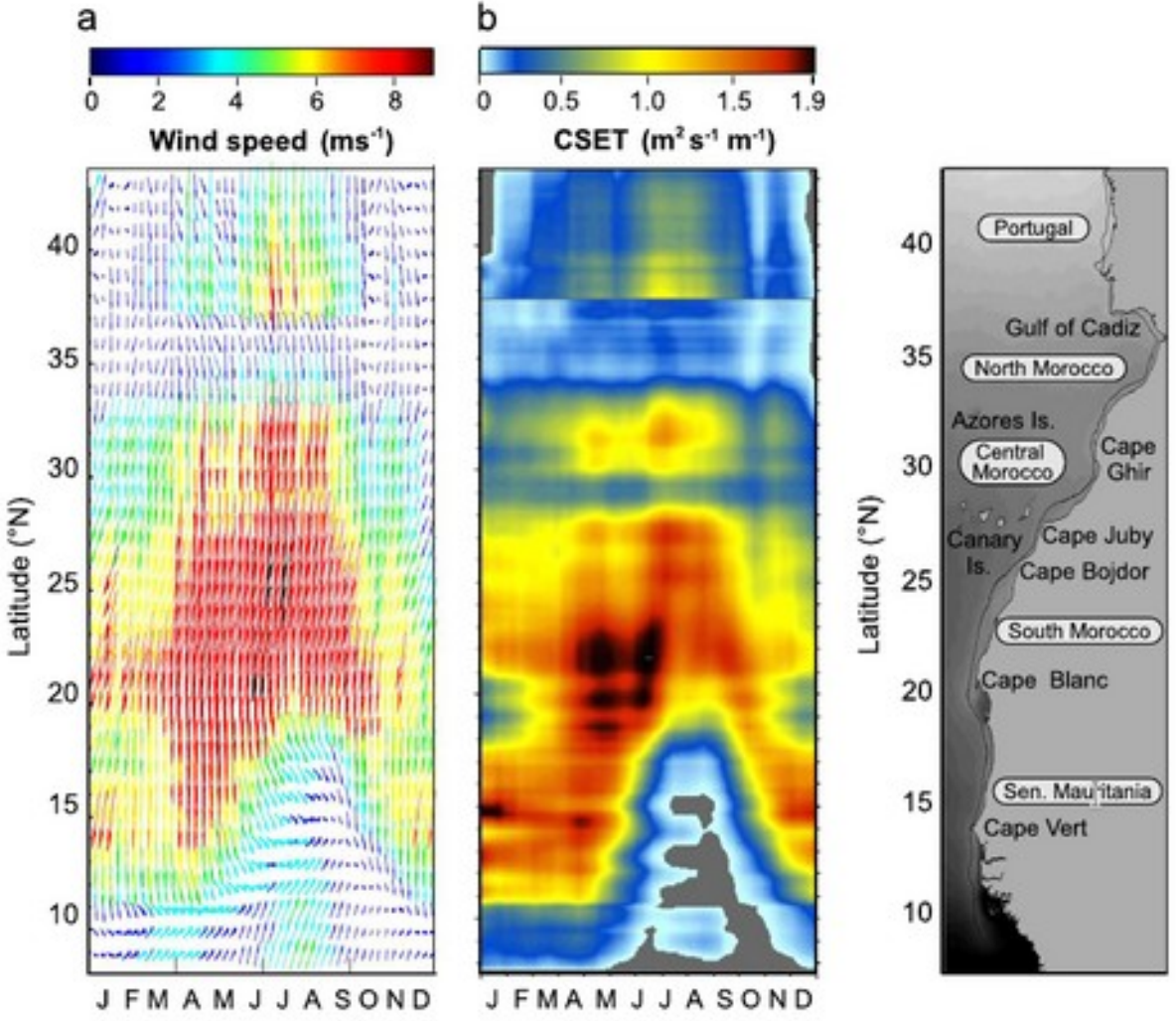

Fig. 4. (a) Climatological mean (8-day averages) of the CCMP satellite wind speed and direction, averaged from 50 to 150 km from the coast, for the period 1988–2010, (b) associated Cross-Shore Ekman Transport (CSET). The break at 37°N is due to the E–W coastline orientation of the northern part of the Gulf of Cadiz.

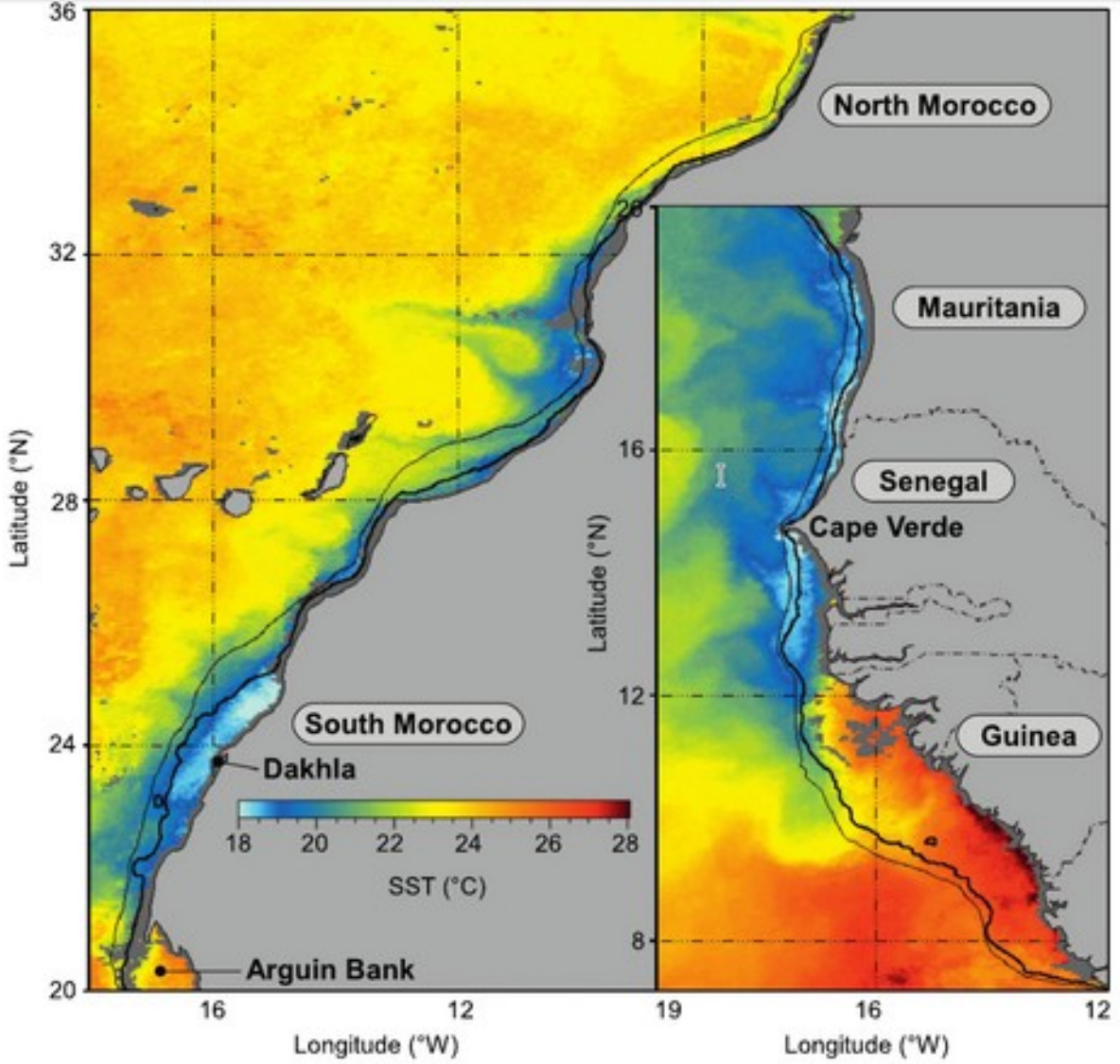

Fig. 3. 8-Day SST composites showing the spatial structure of the coastal upwelled waters in the Moroccan region (left panel) and in the southern part of the system, respectively in 01–08 August 2003 and 1–8 March 2006. The 50 m (thick line) and 200 m (thin line) isobaths are superimposed.

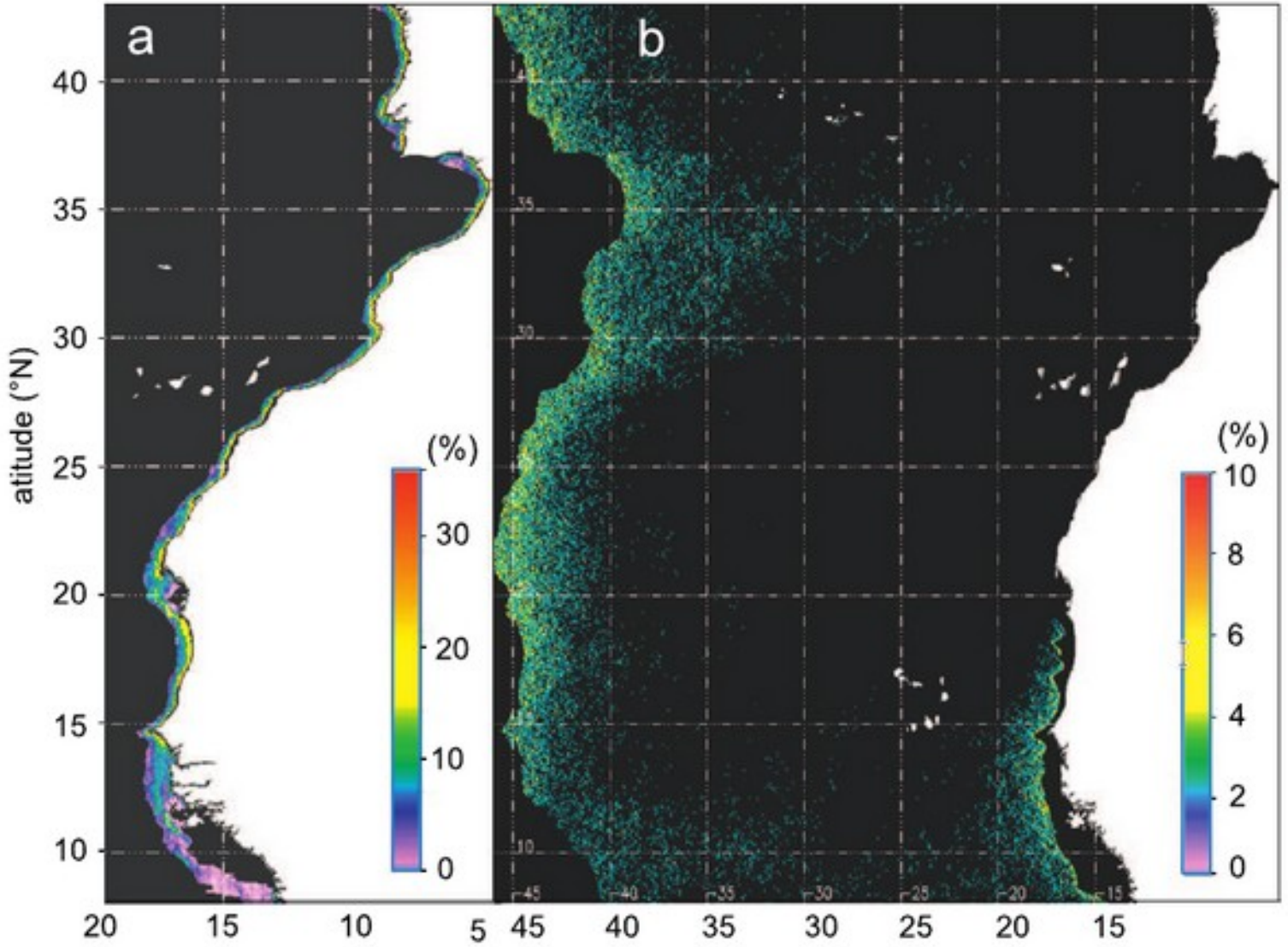
a
b
40
35
30
25
20
15
10
atitude (°N)
(%)
30
20
10
0
(%)
10
8
6
4
2
0
20
15
10
5
45
40
35
30
25
20
15

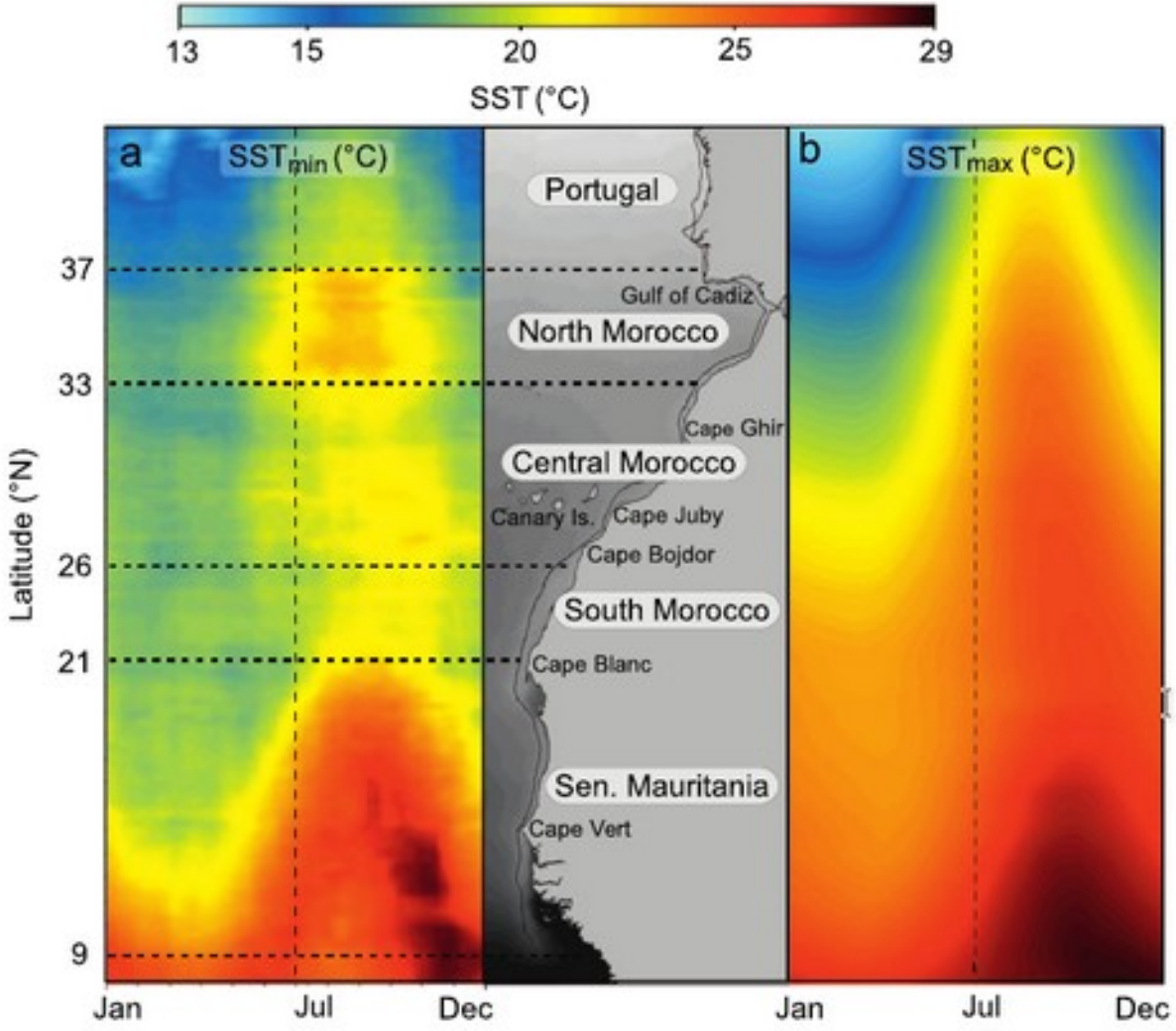

Fig. 8. (a) Space-time Hovmoller plot of the average values of the SST_{min} and (b) the SST_{max} recorded from 1981 to 2011and used for the CUI_{SST} index.

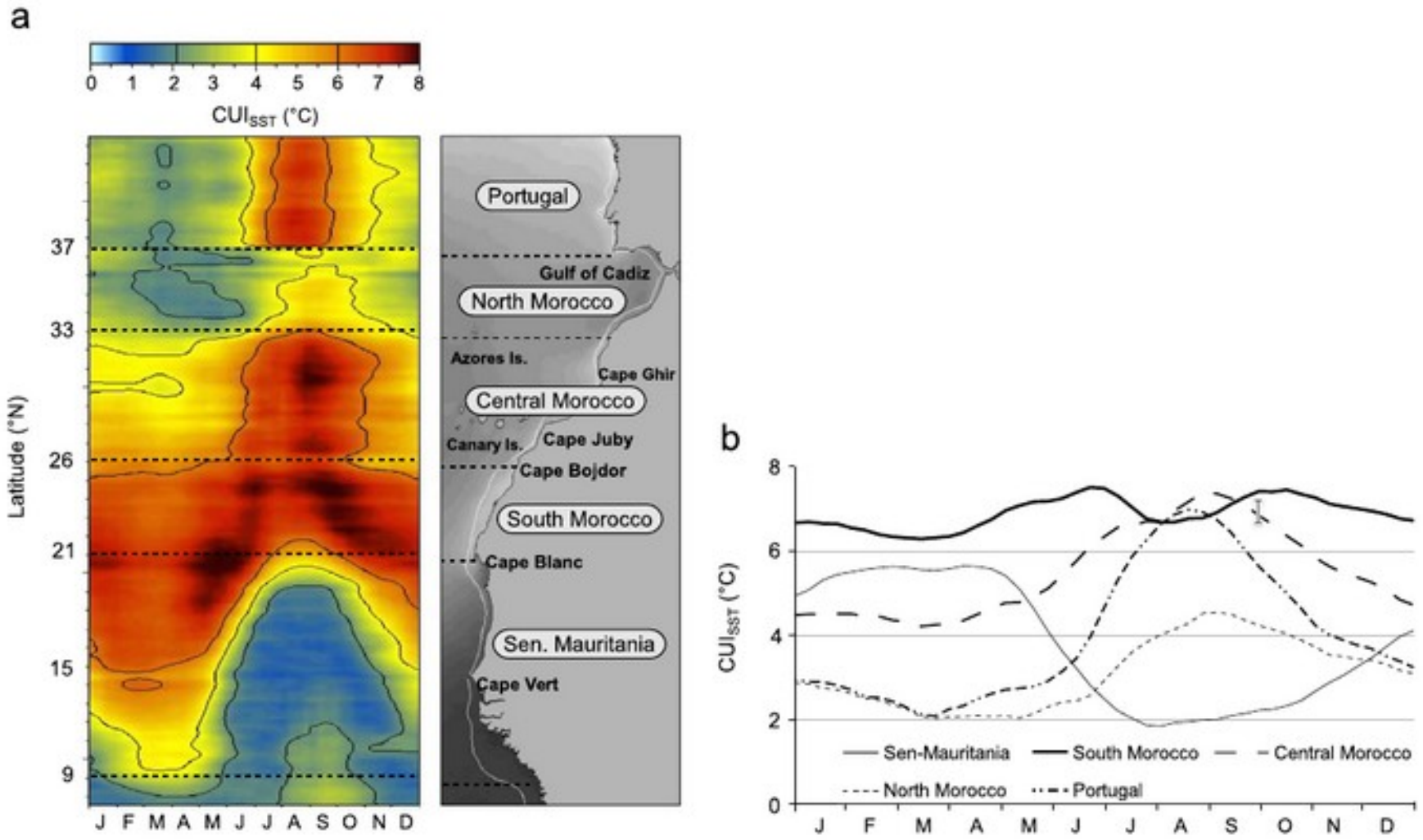

Fig. 9. (a) Space-time Hovmoller plot of the CUI_{SST} index computed from the 1981–2011 time series. Values 2, 4 and 6 °C are contoured. (b) Seasonal variability (three weeks moving average) of the CUI_{SST} index for the five characteristic areas (Portugal: 37.5–43°N, North Morocco: 33–36°N, Central Morocco:26–33°N, South Morocco: 21–26°N and Senegal–Mauritania: 9–21°N) of different intensity and seasonality of the index.

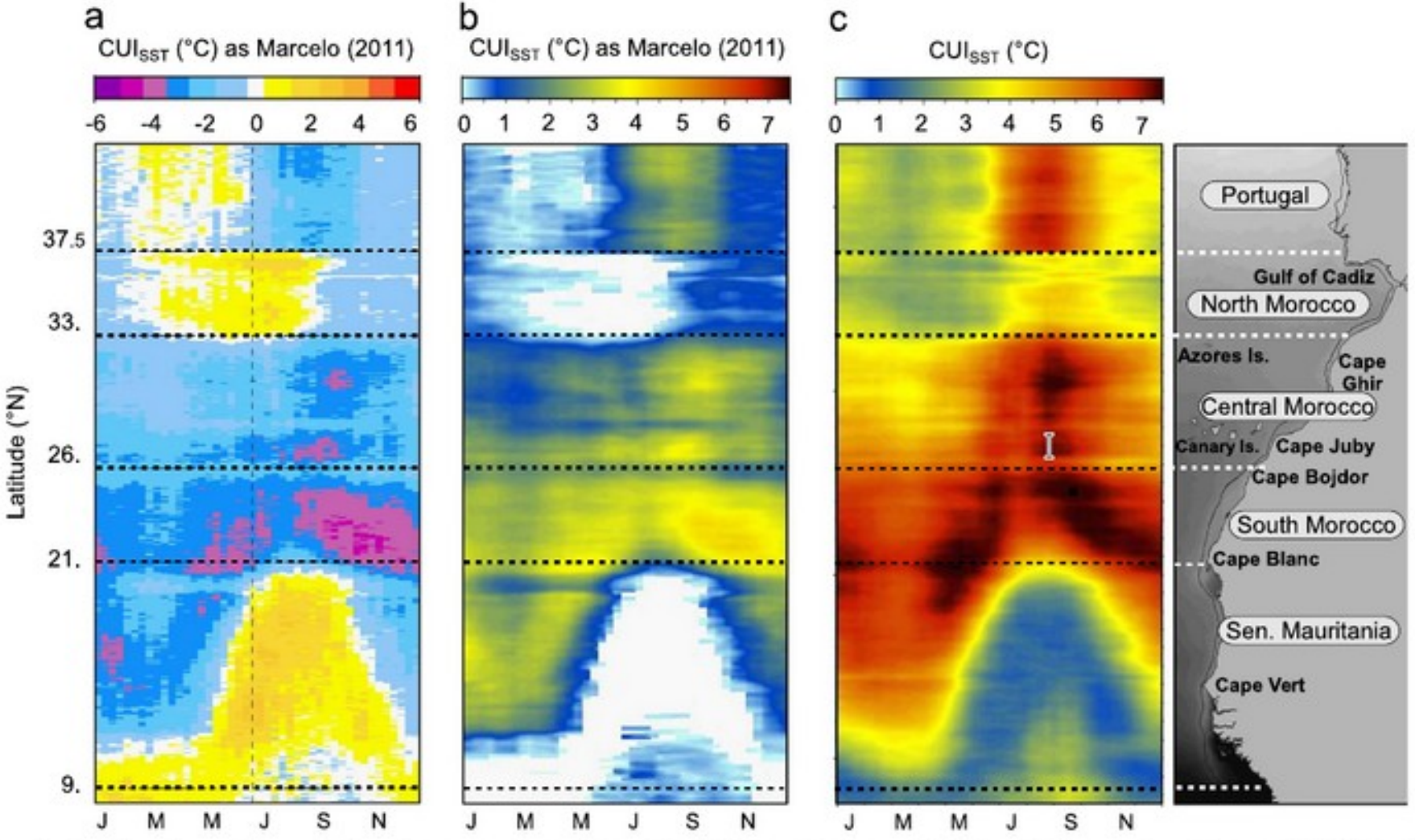

Fig. 10. Climatological Coastal Upwelling Index based on coastal and offshore SST difference for the period (1987–2006) as produced by Marcello (2011) with (a) their original colors (b) enhanced colors with negative values in white and (c) computed with our own methodology, with the same scale and colors.

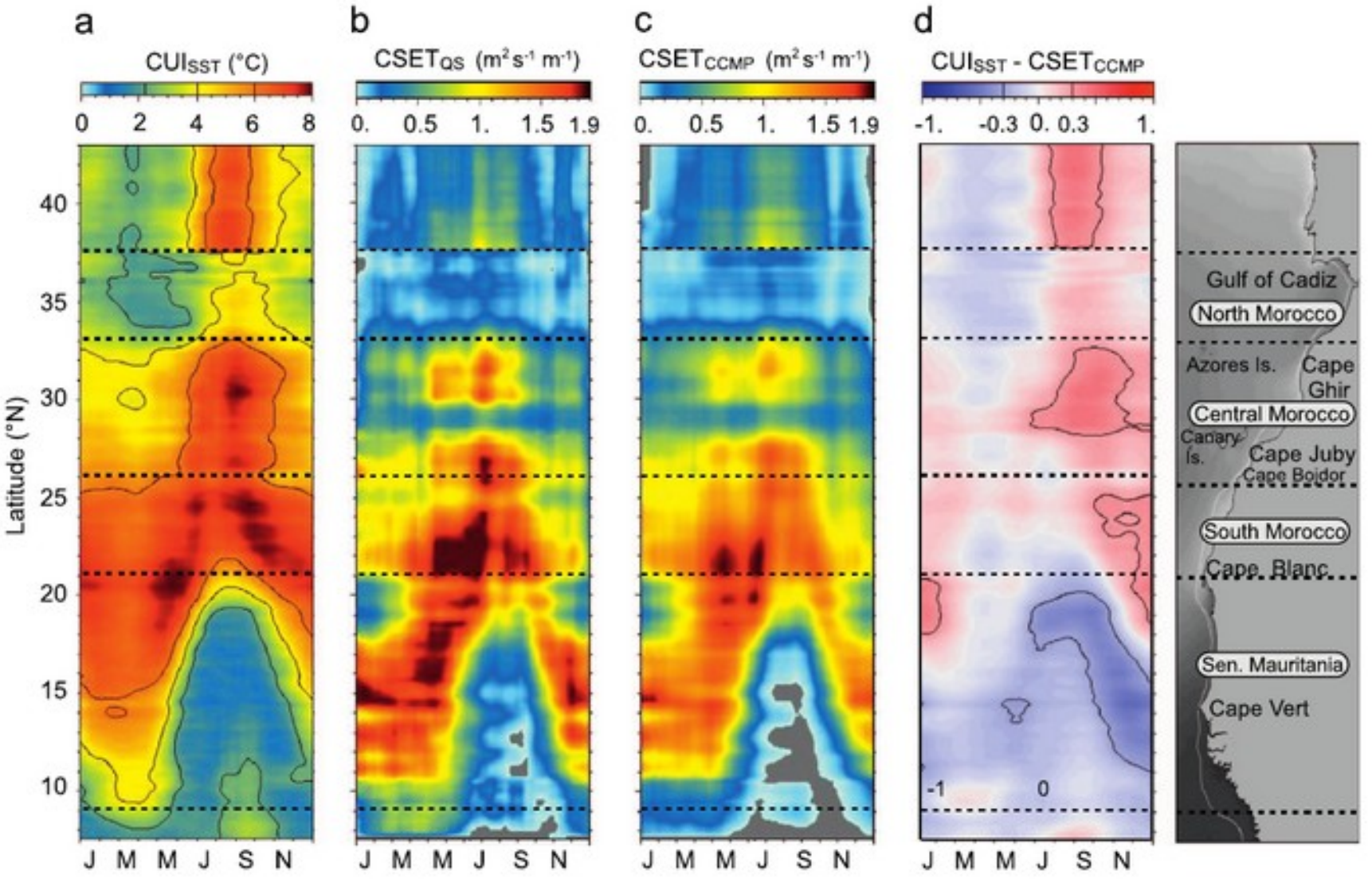

Fig. 11. Seasonal variability of (a) CUI$_{SST}$, (b) and (c) CrossShore Ekman Transport (CSET) computed respectively from QuikSCAT and CCMP winds, (d) normalized differences between CUI$_{SST}$ and CUIC$_{CMP}$.

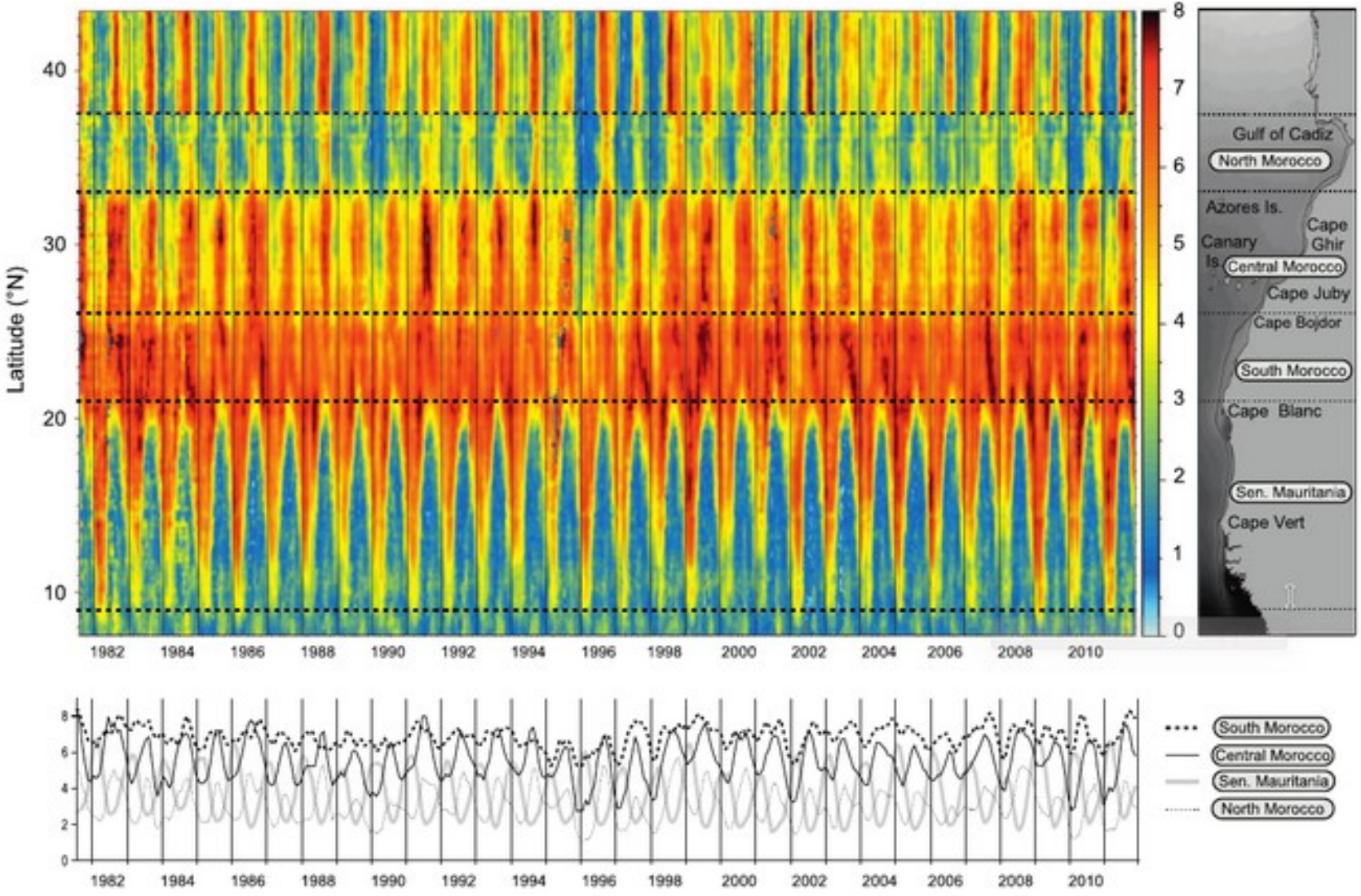

Fig. 14. Space-time Hovmoller plot of the seasonal and interannual variability of the CUI_{SST} (upper panel) from 1982 to 2011 and monthly time series of the four characteristic areas previously identified. (lower panel).

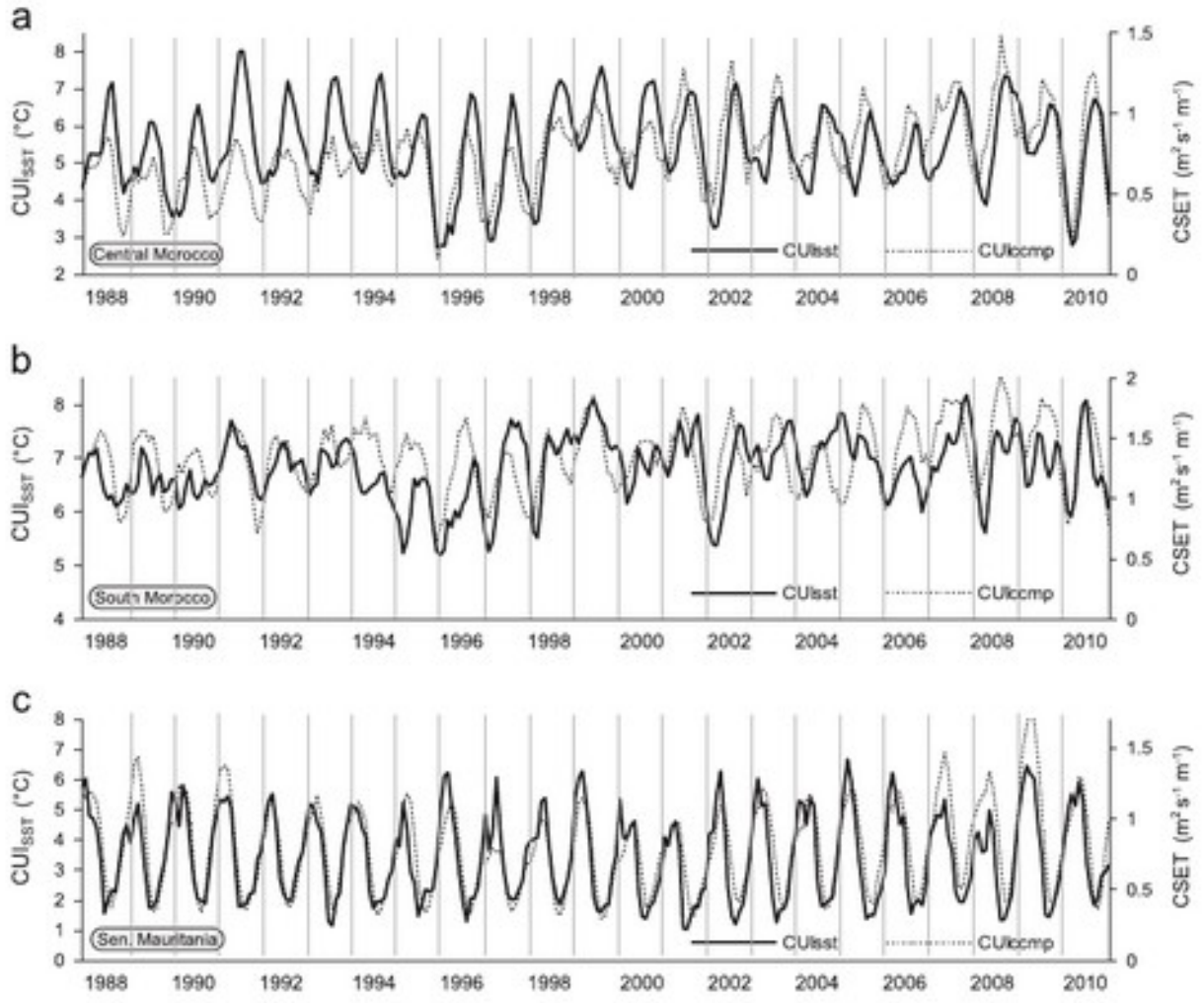

Fig. 15. Comparative seasonal and interannual variability of the CUI_{SST} (plain lines) and the CSET from the CCMP wind (doted lines) from 1988 to 2010 for three contrasted areas: (a) Central Morocco, (b) South Morocco and (c) Senegal–Mauritania. The time step is monthly and the CSET is 3-term averaged.

Taylor & Francis
Taylor & Francis Group

Journal of Operational Oceanography

Year: 2017

ISSN: 1755-876X (Print) 1755-8778 (Online) Journal homepage: http://www.tandfonline.com/loi/tjoo20

The Copernicus Marine Environment Monitoring Service Ocean State Report

Karina von Schuckmann, Pierre-Yves Le Traon, Enrique Alvarez-Fanjul, Lars Axell, Magdalena Balmaseda, Lars-Anders Breivik, Robert J. W. Brewin,

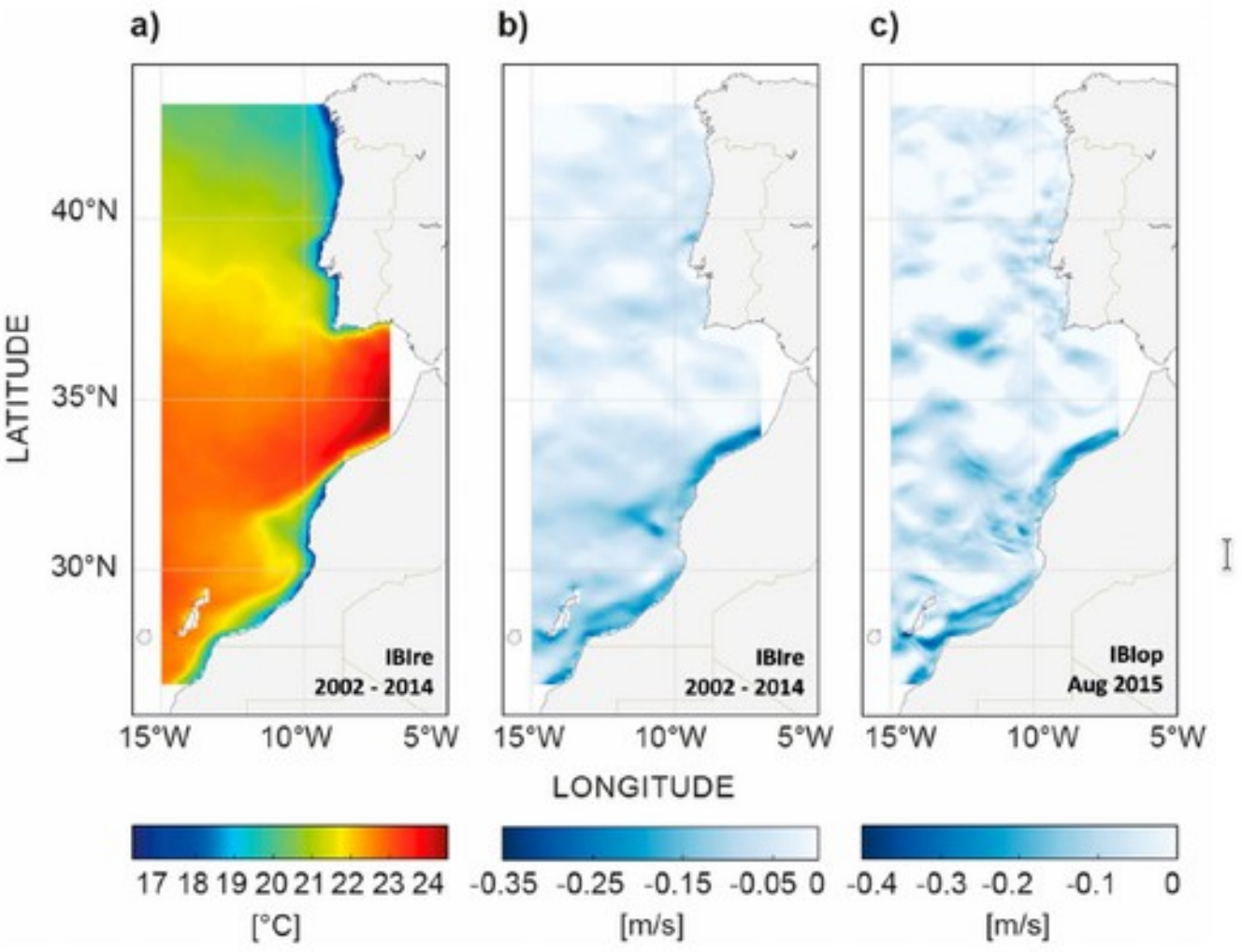

Figure 46. (a) August SST climatology derived from the IBI Reanalysis product (reference period: 2002–2014). (b) Surface Zonal Velocity (positive values not shaded): August climatology derived from IBI Reanalysis (reference period: 2002–2014) (bc) and (c) monthly field for August 2015 from the IBI operational near-real-time Forecast Service (cd). See text for more details on data use.

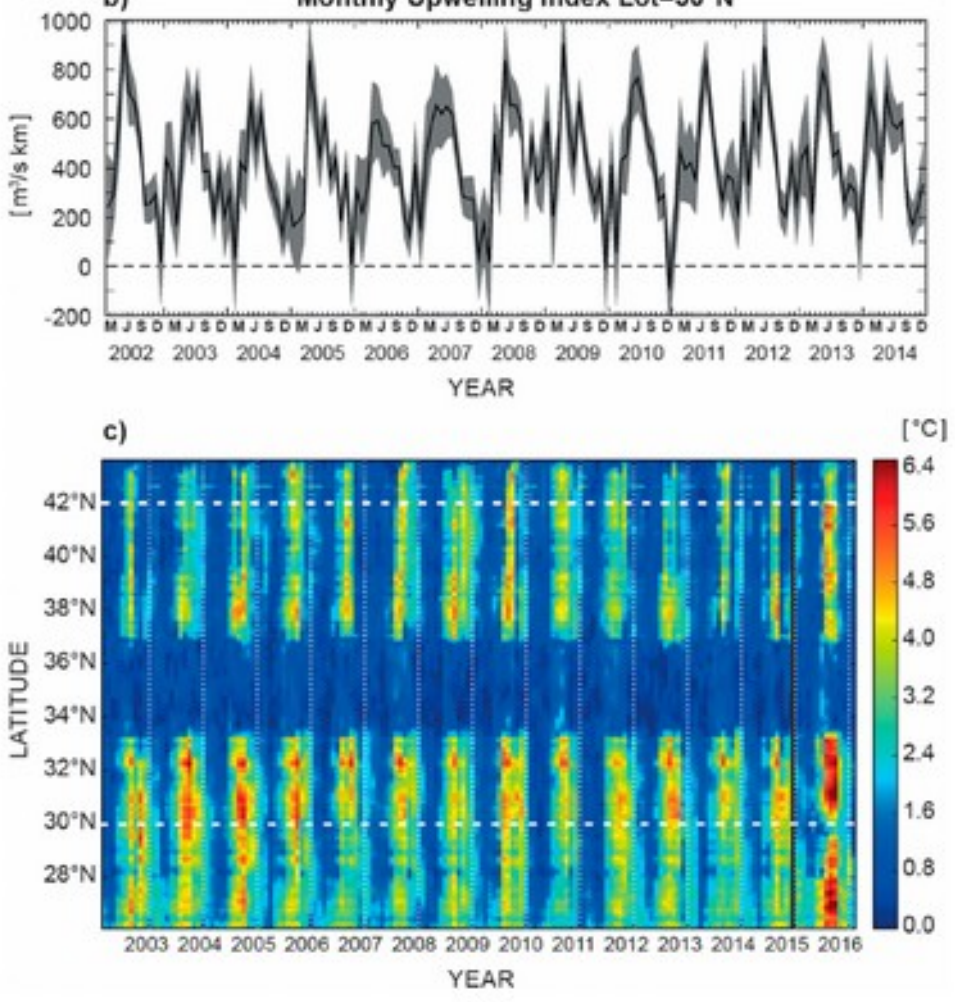

Figure 47. IBI CUIs: (a) and (b) Time series of CUIEK at 42°N (Western IP coast) and 30°N (NWA coast), respectively. CUIEK Index derived from estimation of Ekman transport perpendicular to shoreline of atmospheric forcing of the CMEMS IBI reanalysis. (c) CUISST, zonal Hovmöller diagram. CUISST Index derived from the CMEMS IBI reanalysis data for the 2002–2014 period and from the CMEMS IBI Forecast & Analysis service for the year 2015 (see text for more details on data use). The vertical black line limits the use of both datasets. White horizontal dashed lines denote the latitudes 42°N and 30°N, where CUIEK time series are shown in panels (a) and (b).

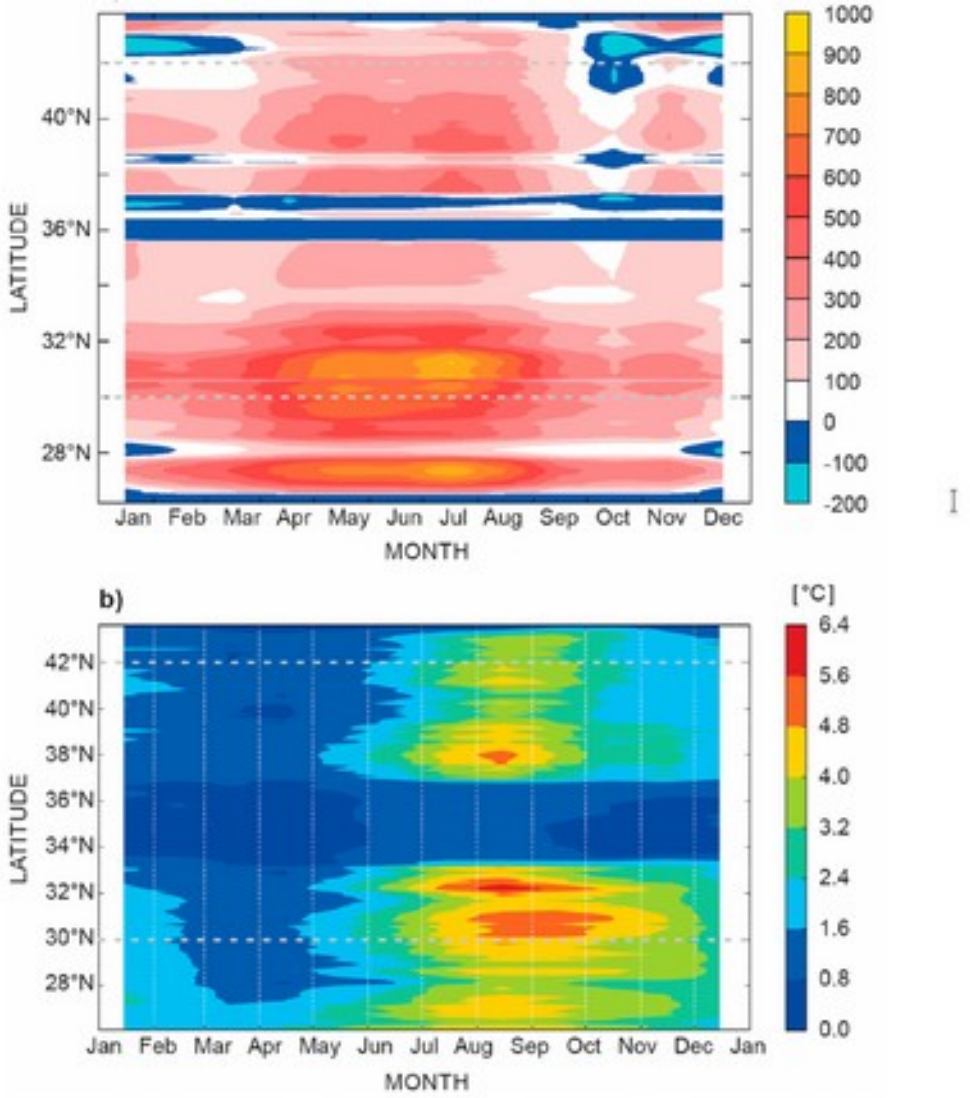

Figure 48. Averaged monthly CUIek (a) and CUISST (b) indexes, contoured by latitude and month. Reference period: 2002–2014 (the CMEMS IBI reanalysis time coverage). Grey horizontal dashed lines denote the latitudes 42°N and 30°N, where CUIEK time series are shown.

Thank you

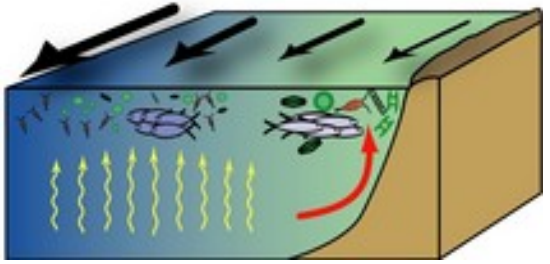

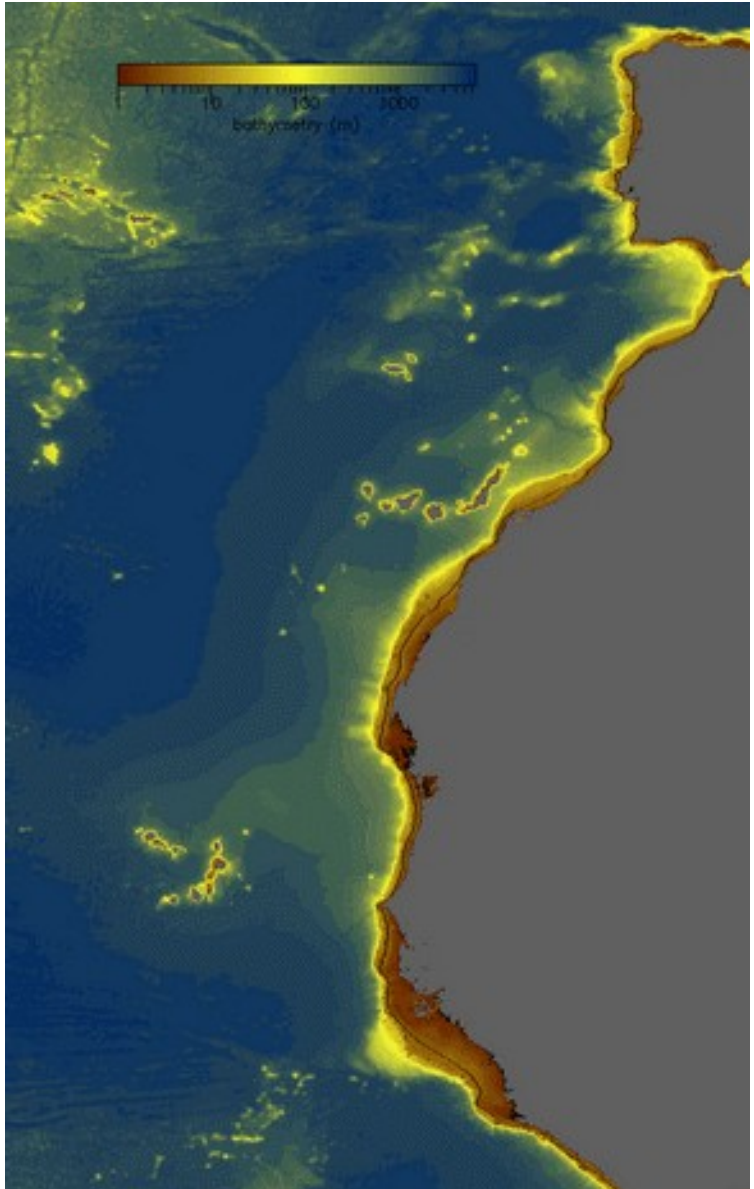
10
100
3000
bathymetry (m)

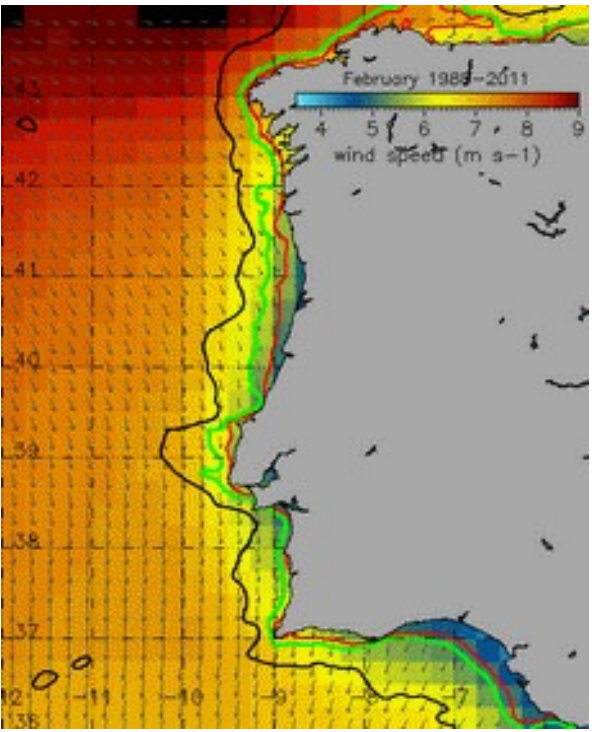
February 1988–2011
4 5 6 7 8 9
wind speed (m s−1)

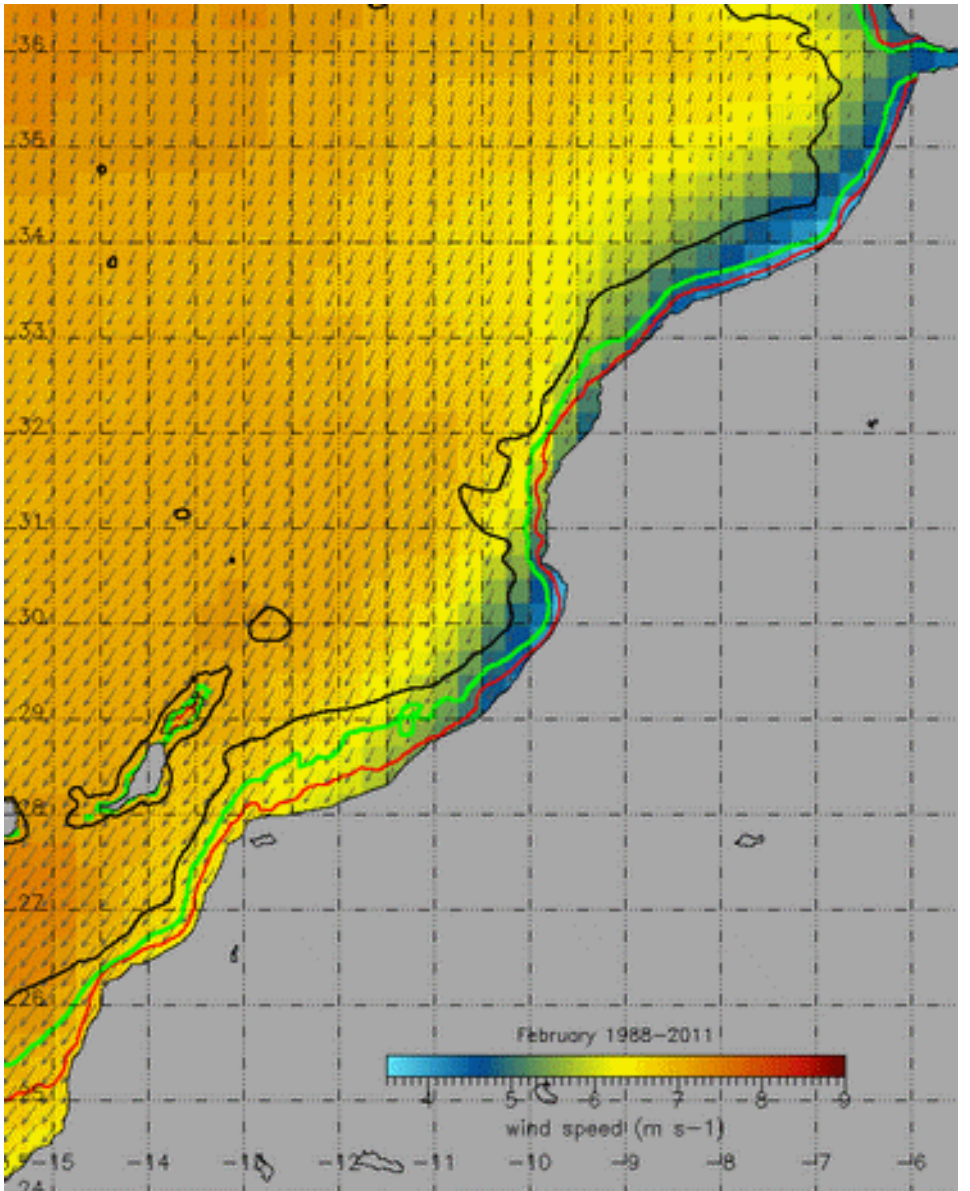
February 1988–2011
4 5 6 7 8 9
wind speed (m s−1)

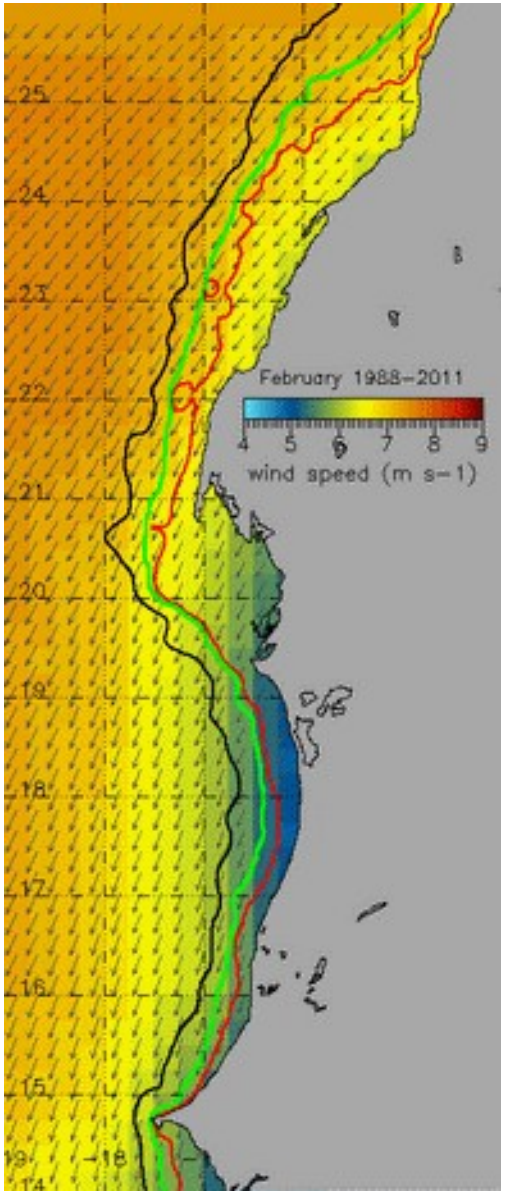
February 1988–2011
4 5 6 7 8 9
wind speed (m s−1)

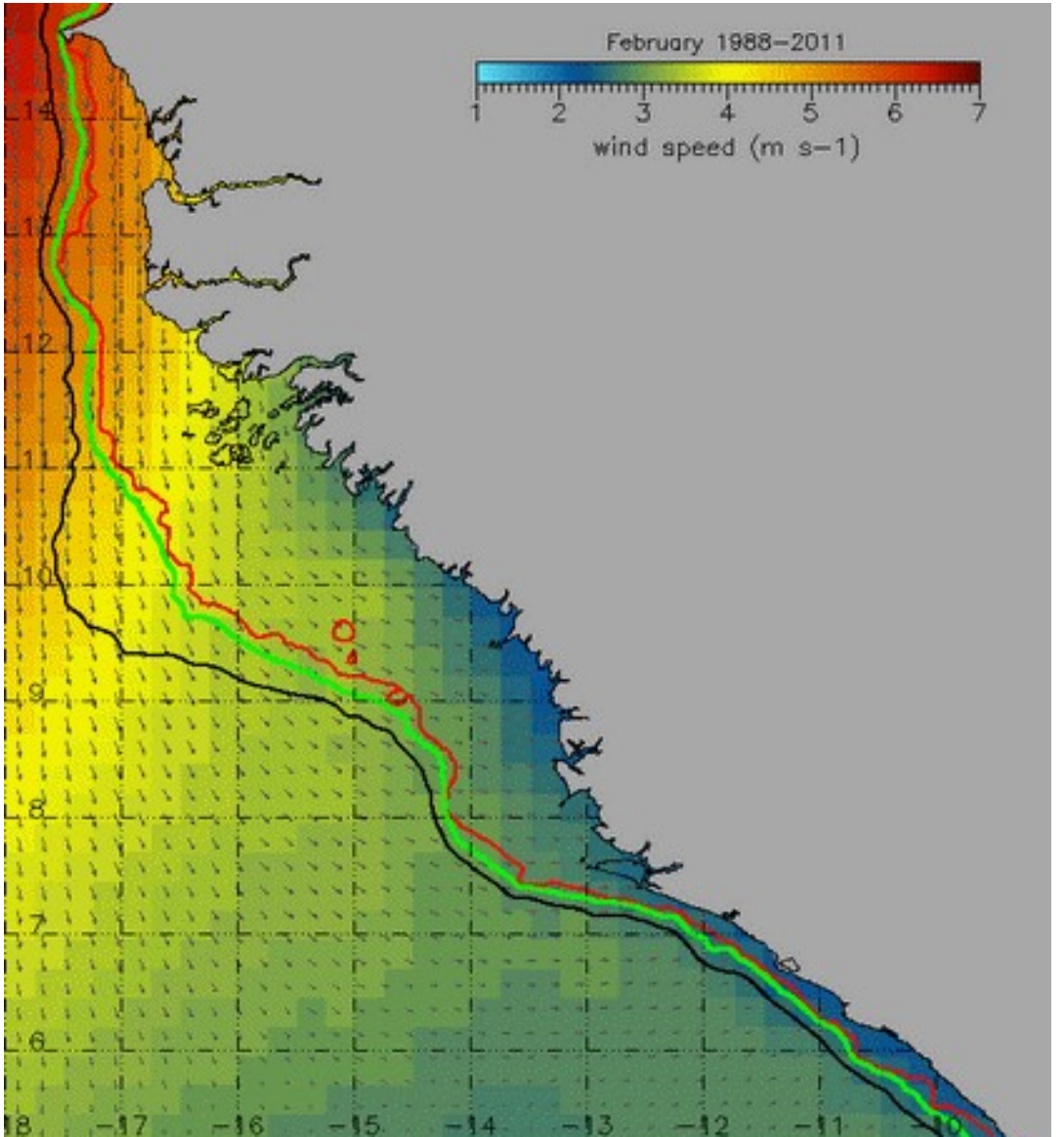
February 1988–2011
1
2
3
4
5
6
7
wind speed (m s−1)
14
13
12
11
10
9
8
7
6
−18
−17
−16
−15
−14
−13
−12
−11
−10

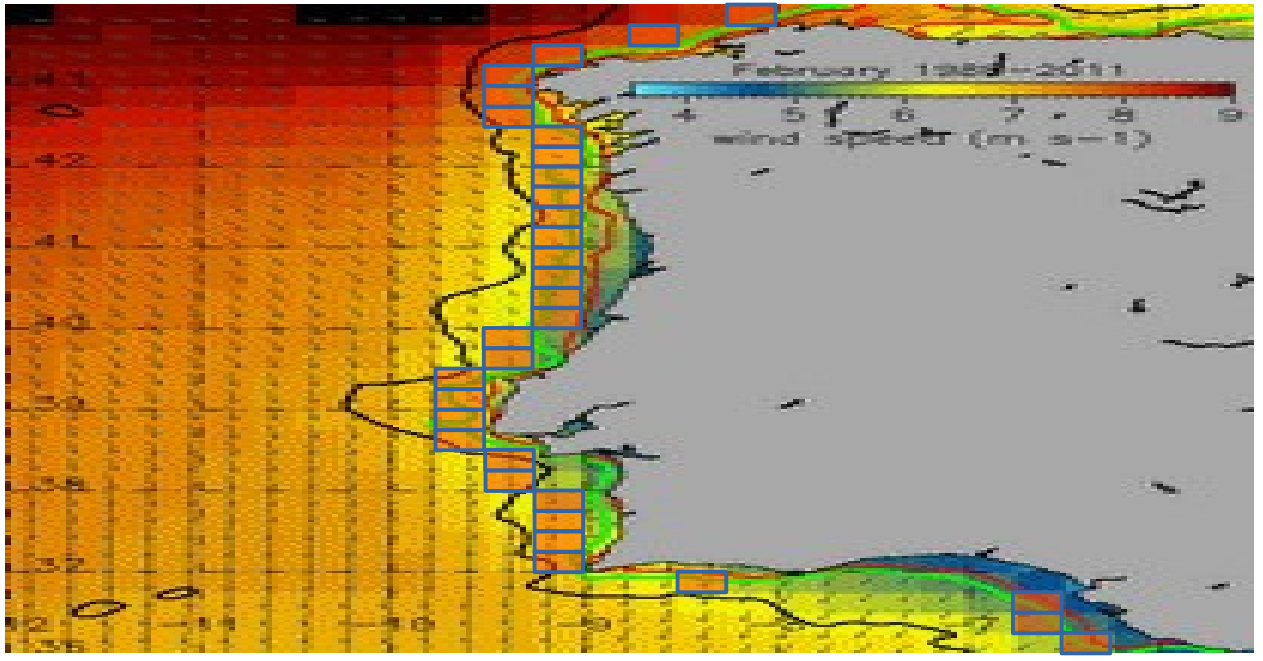
February 1988–2011
4
5
6
7
8
9
wind speed (m s−1)

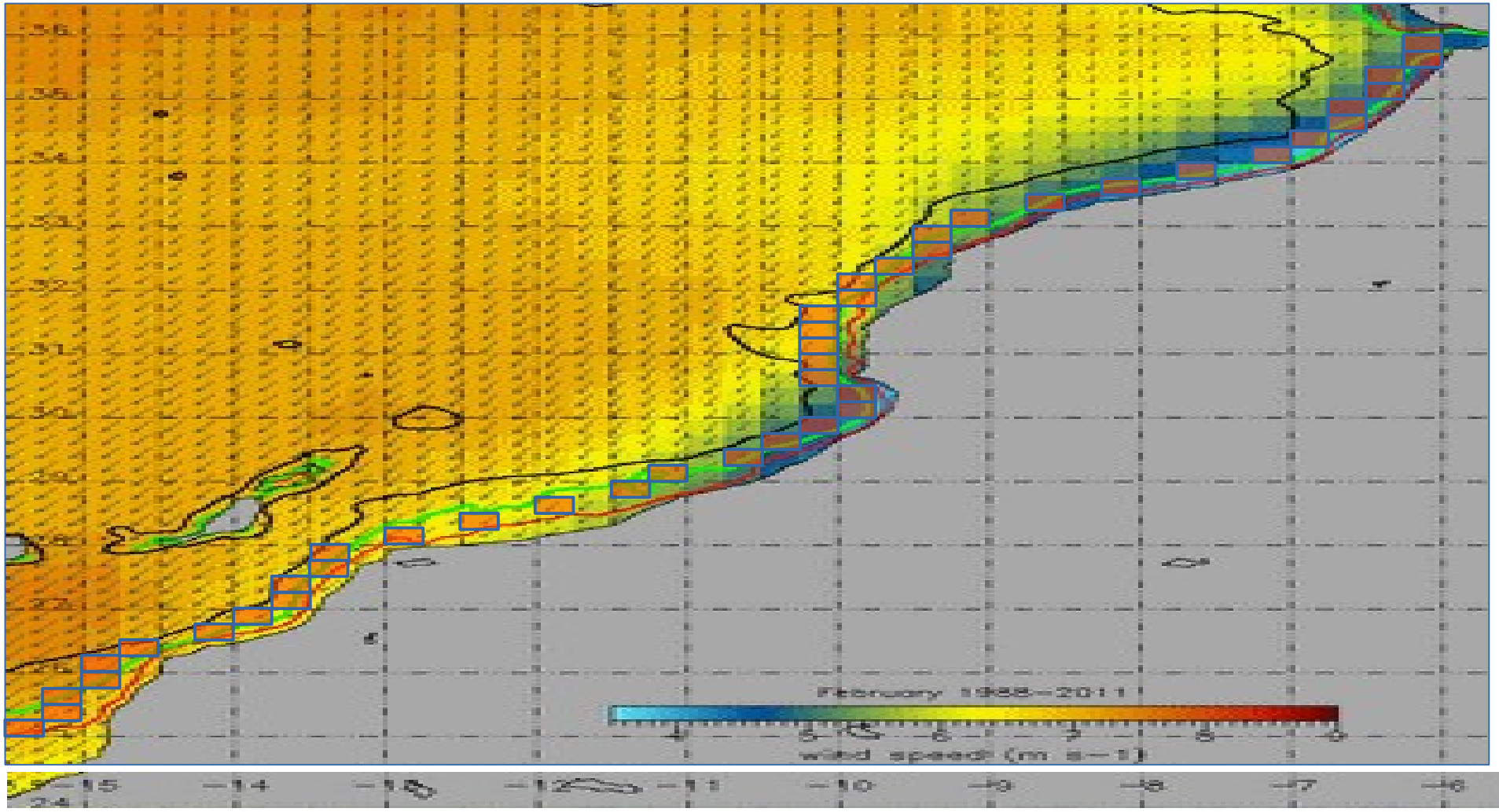
February 1988–2011
wind speed (m s−1)

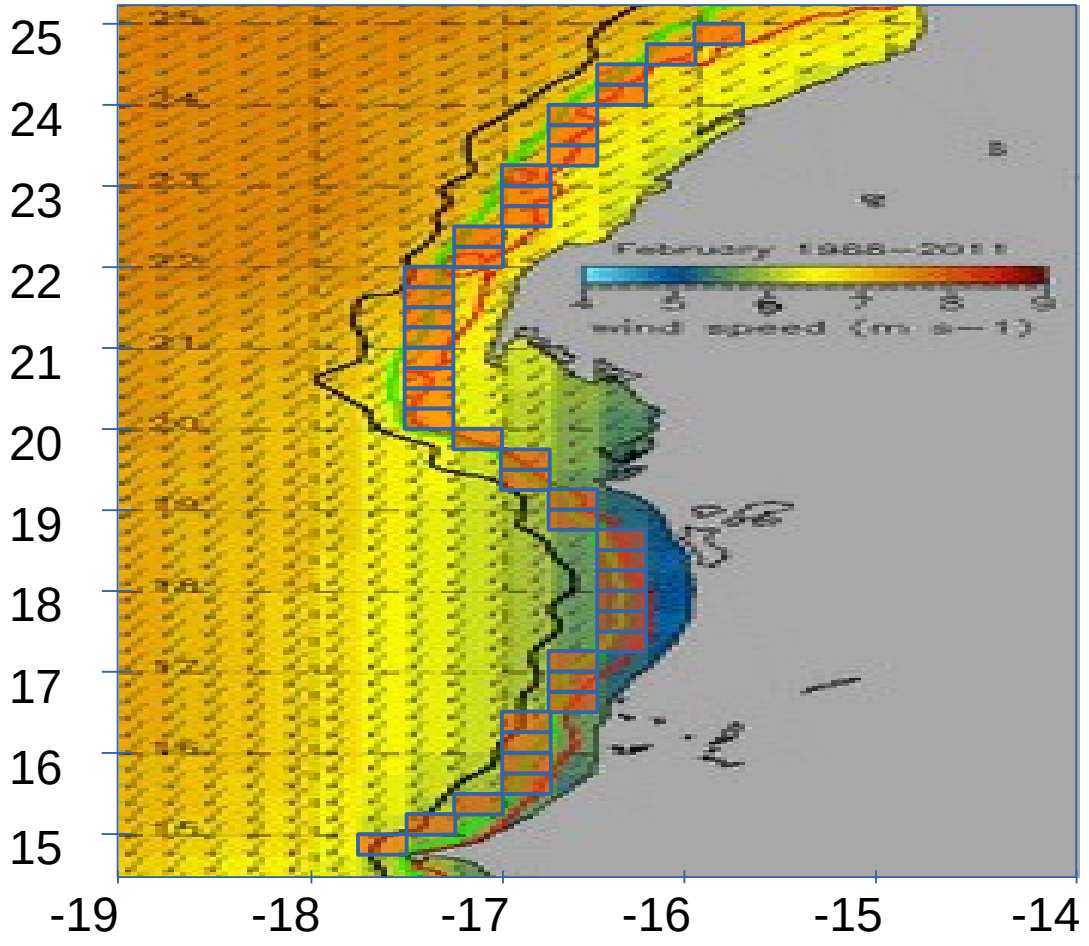
25
24
23
22
21
20
19
18
17
16
15
-19
-18
-17
-16
-15
-14
February 1988–2011
wind speed (m s−1)

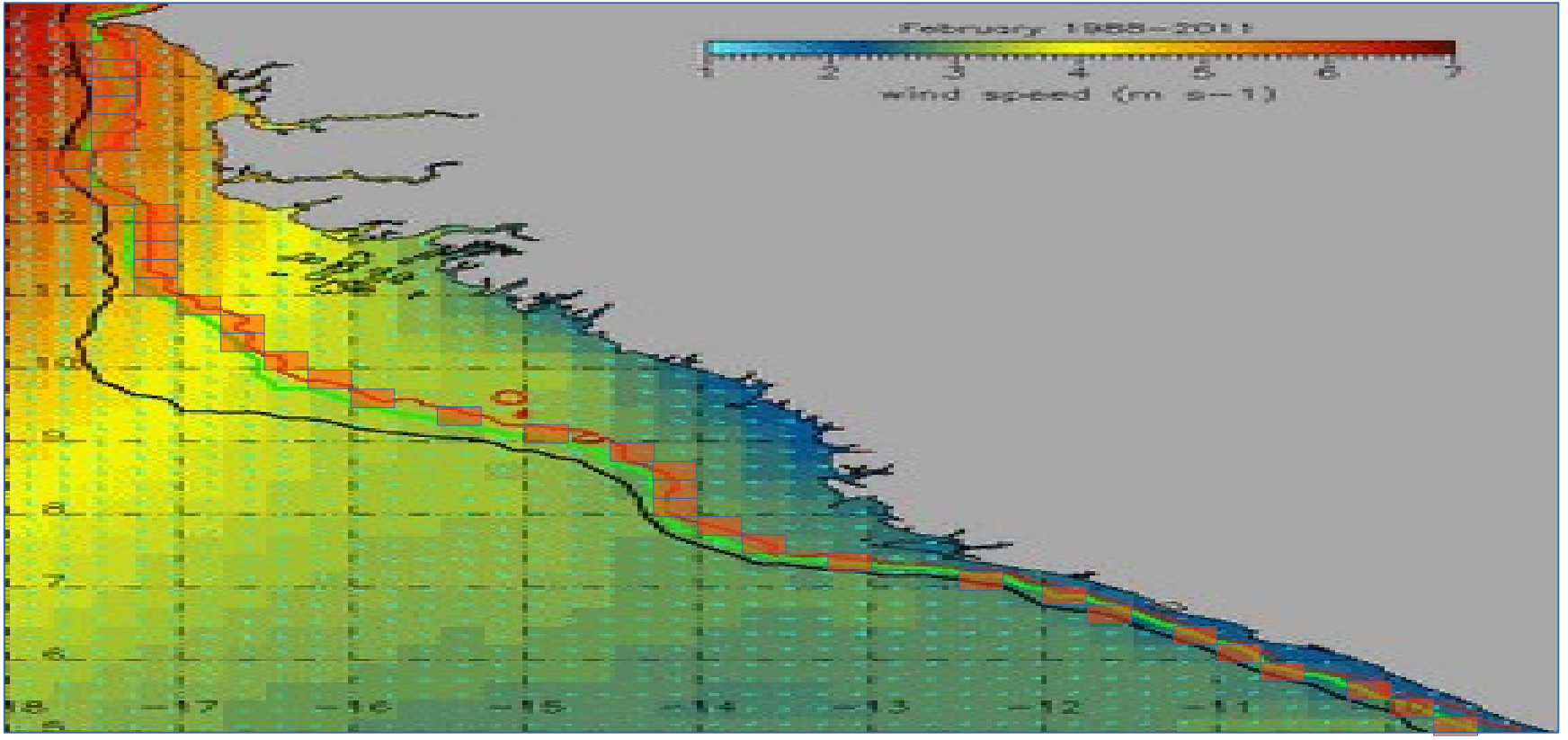
February 1988–2011
1
2
3
4
5
6
7
wind speed (m s−1)
−17
−16
−15
−14
−13
−12
−11